FINAL MASTER PROJECT
MASTER IN ENVIRONMENTAL ENGINEERING AND SUSTAINABLE ENERGY

Modelling of quantitative microbiological risk assessment in bathing waters

By Sarah Munschke

Company Supervisor: Carmen Torres Costa
URV Tutor: Carmen Torres Costa

Tarragona, June 2024

Table of Contents

INDEX

Nomenclature

°C	Degree Celsius
AdV	Adenovirus
AEMET	Agencia Estatal de Meteorología (Spanish State Meteorological Agency)
CFU/100 ml	Colony forming units per 100 ml
CO_2	Carbon Dioxide
COSMO	Consortium for Small-scale Modelling
CSO	Combined Sewer Overflow
D	Diffusion Coefficient
E. coli	*Escherichia coli*
FIB	Faecal Indicator Bacteria
IPCC	Intergovernmental Panel on Climate Change
K	Degradation Rate
k_{pH}	Degradation Rate related to pH
$k_{temperature}$	Degradation Rate related to Temperature
$k_{uv\_intensity}$	Degradation Rate related to UV Intensity
m	Meters
N	North
NE	Northeast
NoV	Norovirus
pH	Potential of Hydrogen
QMRA	Quantitative Microbiological Risk Assessment
SE	Southeast
SSP	Shared Socioeconomic Pathway
UV	Ultraviolet
v_x	Velocity Component in x-direction
v_y	Velocity Component in y-direction
WHO	World Health Organization
W/m^2	Watts per square meter

Summary

This thesis focuses on the modelling of quantitative microbiological risk assessment (QMRA) in bathing waters, with a specific case study on Bogatell beach in Barcelona. The study is motivated by the increasing frequency of extreme weather events due to climate change, which can lead to the contamination of water bodies by microbial pathogens from faecal matter and pose a risk to human health.

The objectives of this thesis are to develop a QMRA tool in Python to assess the risk of waterborne diseases following Combined Sewer Overflow (CSO) events, considering various environmental conditions like temperature, pH, salinity, and UV radiation. This tool aims to assist local authorities and beach managers in making informed decisions about beach safety after CSO events.

Firstly, using Python the distribution of Faecal Indicator bacteria (FIB) such as *E. coli* and *Enterococci* is simulated under consideration of environmental factors for each season and their impacts on pathogen degradation. Secondly the QMRA is conducted to assess the risk for children or adults swimming as well as people participating in recreational activities on the water such as kayaking or rowing.

The results indicate that the pathogen distribution and associated health risks vary depending on seasonal changes in environmental conditions and sea currents, although the speed and direction of the currents has been shown to have the biggest impact.

Based on the outcomes of the simulation and risk assessment potential impacts of the progressing climate change have been discussed as well.

In conclusion, the developed QMRA tool provides a basis for assessing the risks of waterborne diseases in bathing waters after CSO events, contributing to improved public health safety and sustainable water management practices. The focus on Bogatell beach shows the potential utility in real-world scenarios and emphasizes the importance of predictive modelling and risk assessment in the decision-making processes for public health.

1. INTRODUCTION/BACKGROUND

With progressing Climate Change the frequency of extreme weather events including heavy rains and floodings will likely increase and along with it the potential contamination of water sources [1]. The release of untreated wastewater into natural water bodies can lead to potential microbial contamination. Microbial pathogens from faecal matter can cause gastrointestinal diseases which can possibly be deadly [2]. Antibiotic resistance is a growing threat so targeting the causes of infections is becoming increasingly important [1]. Aside from gastrointestinal diseases infections of skin, ear and sinuses are possible as well [3].

Barcelona has a population of roughly 1,6 million inhabitants [4] living on an area of 100 km^2, making it the second biggest city in Spain [5]. Due to its high population density the maintenance of a working sewer network is very complex. While the total annual amount of rain is moderate and it does not rain often, intense rain events happen which are characteristic for the Mediterranean area [5].

Barcelona uses a combined sewer system, meaning that rainwater and wastewater are transported together [6], in total the sewer system is over 1500 km long [5].

Combined sewer systems have overflow chambers to ensure security during extreme weather events, like heavy rain or floods, which can release excess water into receiving water bodies, in this case the Mediterranean Sea [7]. The sewers handle approximately 300 m^3 a day in dry weather [8]. Combined sewer systems were common in big or fast-growing cities, especially during the 19th and 20th centuries, as they were a fast solution to prevent flooding inside the cities during heavy rain events [6], [9]. Both the effects of climate change and the higher rate of sealed surfaces in cities have since increased the amount of stormwater runoff [9]. While the long-term goal of the planning of the sewer network has been to avoid floodings in the city the number of Combined Sewer Overflows (CSO) was also going to be reduced [5].

In order to prevent uncontrolled floodings during heavy rainfalls Combined Sewer Overflows into adjacent water bodies are used when the system is nearing its overload [9]. Combined Sewer Overflow means that the mix of rainwater and wastewater is released into the sea to relieve the system. One of these overflow points is located in Bogatell beach and releases the water into the Mediterranean Sea.

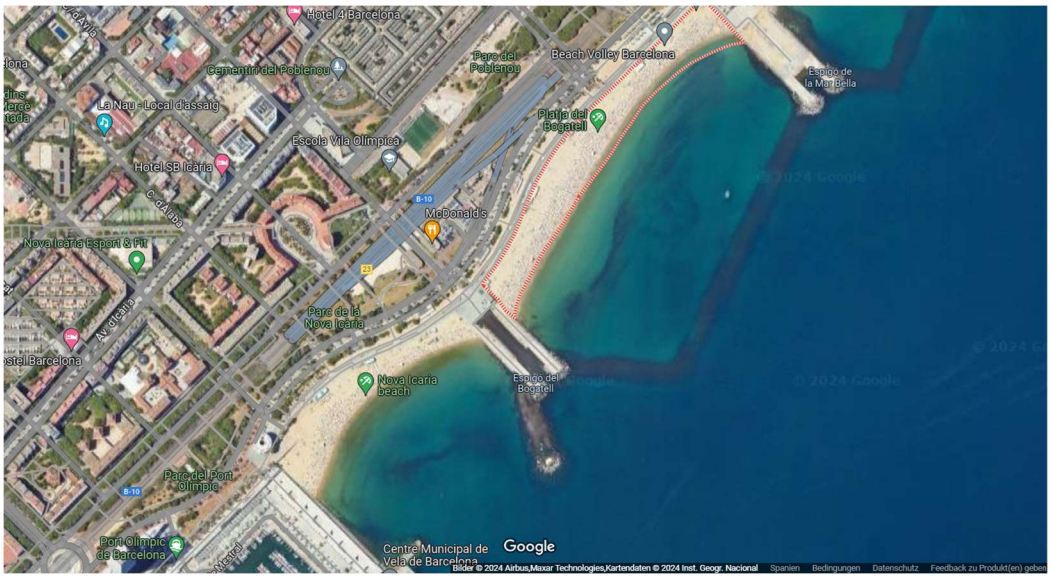

Figure 1: Map of Bogatell beach in Barcelona [10]

Sewage discharges including CSOs are the most common source of microbial contamination of sea waters [11]. The microorganisms contained in the water may pose a risk to the health of beach goers later on.

Gutiérrez et al. [5] describe that in accordance with the European Bathing Water Directive which enforces active management instead of just monitoring water quality, the city of Barcelona has a protocol in place to deal with these short-term contamination episodes. The general public and the beach managers are informed both through electronic panels at the beach and online. The Coastal Water Management system COWAMA is used to predict the bathing water quality for up to 48 hours by modelling based on real time data from different sensors and meteorological predictions [5].

In October 2021 the "Dynamic Information Management Approach for the Implementation of Climate Resilient Adaptation Packages in European Regions" IMPETUS project was founded as part of the European Union's Horizon 2020 Green Deal call to help adapt to Climate Change.

One task of the IMPETUS project is improving bathing water quality in extreme storm events by developing a QMRA model for a demo site, to better predict, monitor and manage the risk of water-borne diseases. It is based on the previous case study on the coast of Barcelona called iBathwater [12]. The goals of the iBathwater project were to reduce pollution levels in water bodies near urban centres, including Barcelona. During this project the water quality during and after CSO events was monitored [13].

1.1. Environmental conditions at Bogatell beach in Barcelona

Since the environmental conditions at the beach will be relevant for the simulation of pathogen degradation later on, here an overview is given on the situation.

The sea surface temperature of the Mediterranean Sea in Barcelona generally varies throughout the year between 12 °C and 26 °C, as is shown in Figure 2.

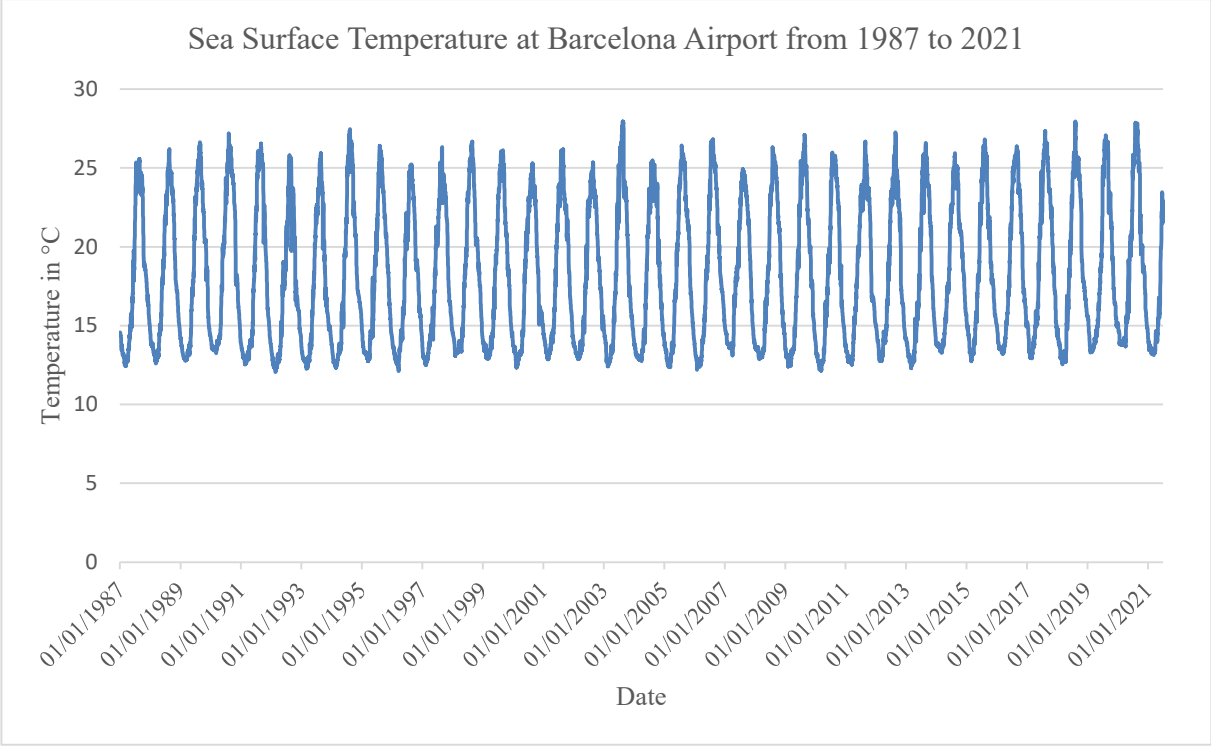

Figure 2: Sea Surface Temperature measured at Barcelona Airport between 1987 and 2021 [14]

The average monthly water temperature in 2022 according to the Instituto de Estadística de Cataluña (Idescat) is shown in Table 1 [15]. The average values displayed here for each season will be used in the simulation later on.

Table 1: Average monthly sea temperature in 2022 (Data: [15])

Month	Temperature (°C)	Average	Season
December	15,4	14,20	Winter
January	13,8		
February	13,4		
March	12,9	14,63	Spring
April	13,9		
May	17,1		
June	21,4	23,50	Summer
July	23,9		
August	25,2		
September	23,2	20,97	Autumn
October	21,4		
November	18,3		

The average solar radiation data was measured daily at the Barcelona airport in 2022 [14]. The monthly averages are shown in Table 2 as well as the associated values used for each season.

Table 2: Average daily solar radiation in W/m^2 in 2022 (Data: [14])

Month	Solar radiation in W/m^2	Average	Season
December	71,94	94,82	Winter
January	82,81		
February	129,71		
March	112,55	200,45	Spring
April	205,77		
May	283,03		
June	294,10	285,39	Summer
July	298,45		
August	263,61		
September	187,10	139,21	Autumn
October	135,42		
November	95,10		

In Figure 3 the daily solar radiation at the airport in Barcelona is displayed throughout the year. The highest radiation occurs during the summer months, usually from May to August, as is also shown in the seasonal average values in Table 2.

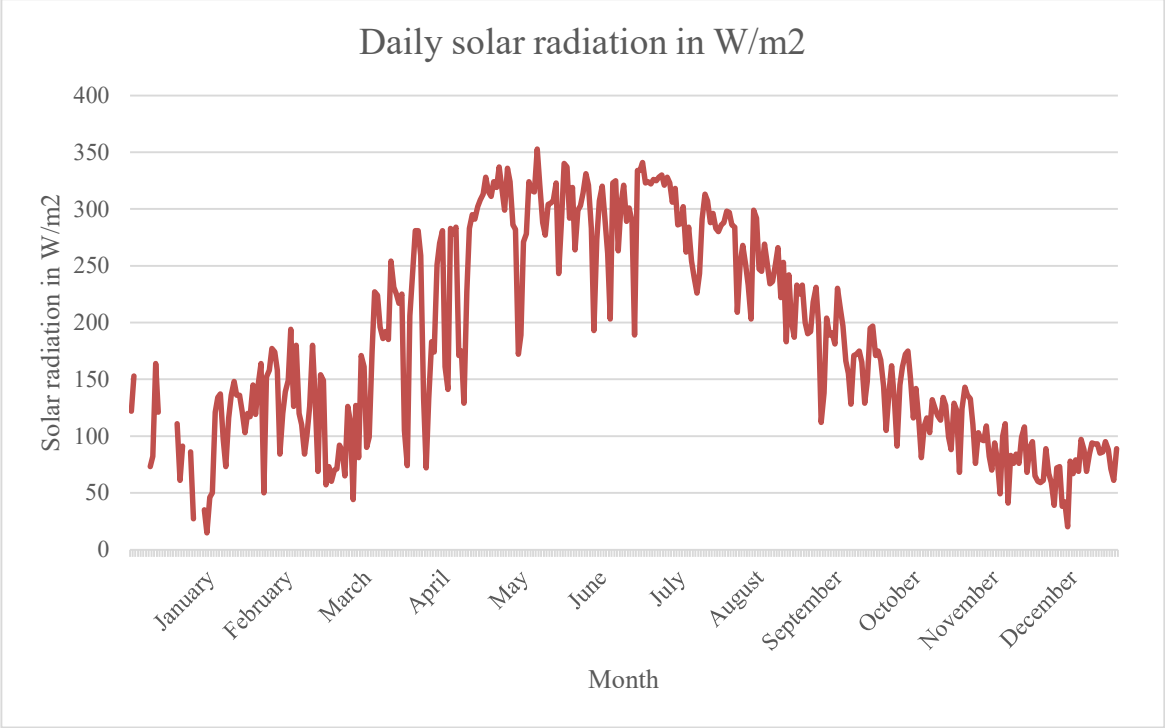

Figure 3: Daily Solar Radiation at Barcelona Airport in W/m^2 (Data: [14])

Figure 4 shows the daily precipitation in mm measured at the airport in Barcelona between 1980 and 2022. The singular days of very heavy rain events throughout the years are clearly visible.

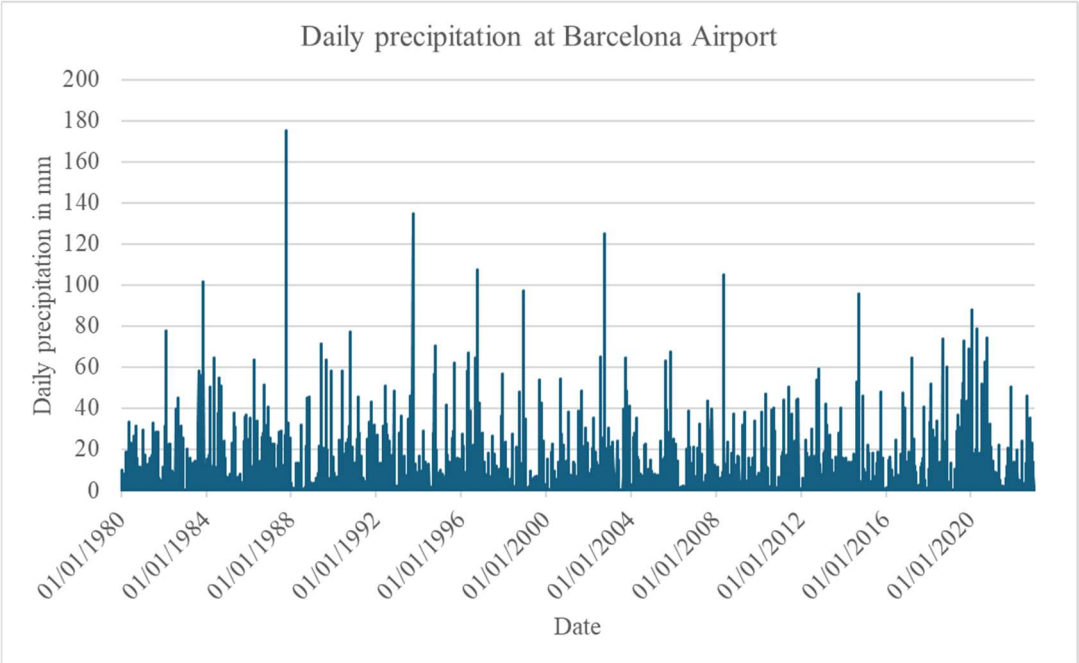

Figure 4: Daily Precipitation measured at Barcelona Airport between 1980 and 2022 (Data: [14])

Figure 5 shows that the salinity at the sea surface varies between 37 and 38,5 ‰ throughout the years. These variations have been consistent throughout the years between 1987 and 2021.

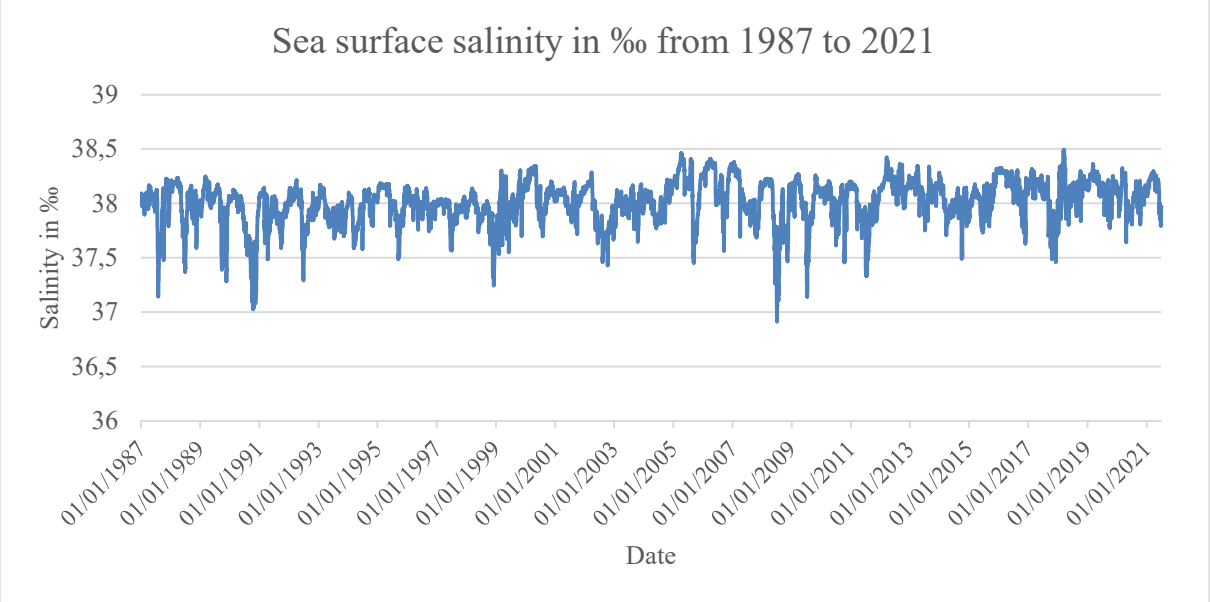

Figure 5: Sea Surface Salinity at the Barcelona Airport between 1987 and 2021 (Data: [14])

For a more detailed view of the changes throughout the year the most recent available data on salinity is used. It is from July 2020 to the end of June 2021 and is shown in Figure 6. Although the changes in salinity are rather small and vary between 37,8 and 38,3 ‰ the average for each season is to be used for the simulation and are displayed in Table 3.

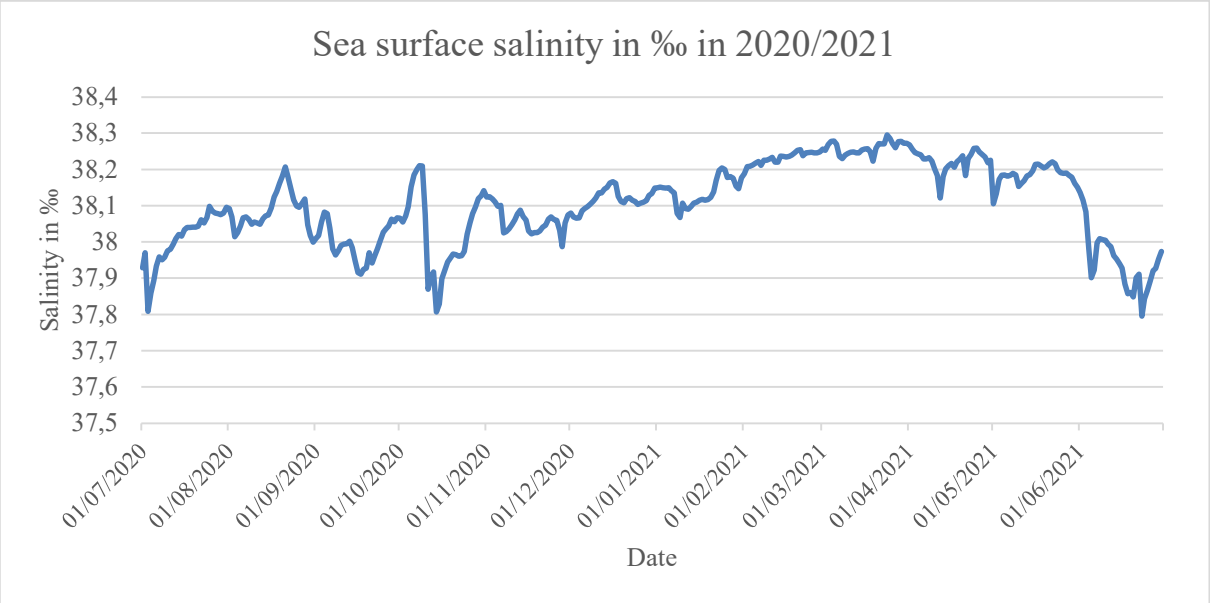

Figure 6: Sea Surface Salinity at Barcelona Airport in 2020/2021 (Data: [14])

Table 3: Average Sea surface salinity values for each season in %

Season	Salinity in %
Spring	3,822
Summer	3,801
Autumn	3,803
Winter	3,816

On a large scale the Catalan Sea, which the area between the Iberian coast and the Balearic Islands is called, contains a permanent south-westward current called the Northern Current, which starts in northern Italy [16].

On a smaller scale the speed and direction of the sea currents in the Mediterranean Sea varies throughout the year. The data for the speed and direction of the currents was taken from the Atlas of surface currents in the Mediterranean [17] and accessed through the COSMO site which provides an electronic version of the data [18]. The study is part of the Interreg Euro-MED program cofounded by the EU [19]. An example of the COSMO site can be seen in Figure 7 for the month of August.

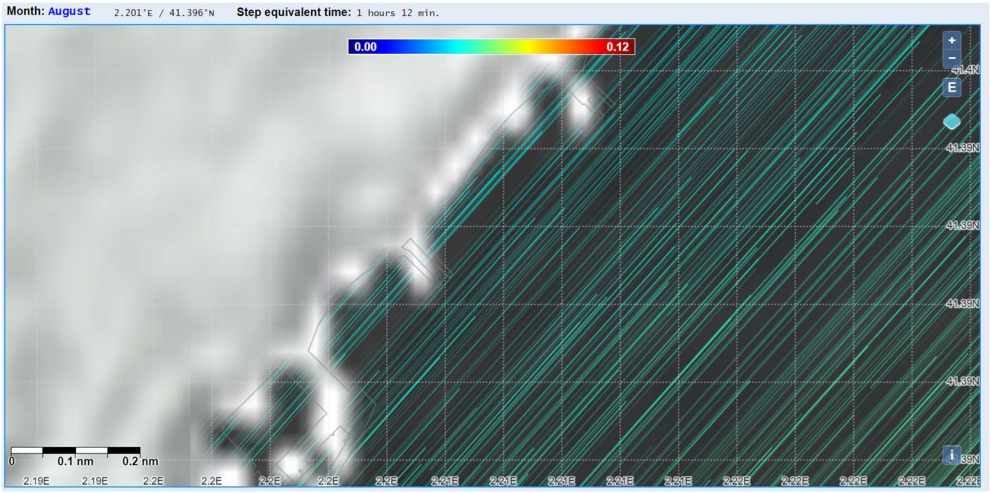

Figure 7: Example of the COSMO site showing the sea currents in August on the coast of Barcelona [18]

The results are shown in Table 4. The direction states where the currents are coming from.

Table 4: Velocity of sea surface currents in Barcelona (Data from COSMO [18])

Month	Velocity (m/s)	Direction
January	0,01	NE
February	-0,01	SE
March	-0,01	W
April	0,04	NE
May	0,06	NE
June	-0,01	SE
July	-0,07	SW
August	-0,11	SW
September	-0,08	SW

October	-0,08	SW
November	0,03	SE
December	0,01	ENE

The average speed and direction of the sea currents that will be used for the simulation will be discussed in chapter 3.3.1.

2. OBJECTIVE AND SCOPE OF THE PROJECT

The objective of this thesis is to develop a Quantitative Microbiological Risk Assessment (QMRA) tool in Python to determine the risk for beach goers stemming from potential pathogen contamination of the bath water following Combined Sewer Overflow (CSO) events. It is supposed to help monitor the consequences of CSO after heavy rain events and to decide when to potentially advise against visiting the beaches when necessary. Not only the distribution of the pathogens is considered but also their degradation depending on the environmental conditions such as pH, temperature, salinity, and UV radiation.

Using Faecal Indicator Bacteria, the pathogens are quantified and the risk for human health is assessed based on these estimations for different scenarios. The outcome of the risk assessment can be used for decision making by local authorities and beach managers to determine when to advise against swimming. The QMRA tool will be developed and validated using data from Bogatell beach in Barcelona.

Research question: How do variations in environmental conditions (pH, temperature, salinity, and UV radiation) affect the distribution and degradation of pathogens in bathing waters following Combined Sewer Overflow (CSO) events, and what is the associated risk to human health?

3. METHODS/APPROACH

3.1. Model structure

The flow diagram in Figure 8 shows how the simulation is going to work. Firstly, general constants like the dimensions of the beach, breakwater and the location of the point source have to be defined as well as the diffusion coefficient and time step size. Secondly, the ratios of Faecal Indicator Bacteria (FIB) to Adenovirus and Norovirus are set, as well as the environmental parameters for each season.

Now the function to calculate the FIB distribution is defined, starting with a validation of all inputs. The parameters are retrieved from the according season and a grid is defined for the calculation. Throughout the time-stepping loop the advection, diffusion and degradation are being calculated for each time step. The degradation calculation is based on the seasonal parameters and uses the degradation rates according to them. After the simulation is completed the distribution of FIB can be plotted. Using the ratios of FIB to pathogens the amounts of pathogens can be determined and used for the following risk assessment.

To conduct the risk assessment the respective dose-response models for each pathogen define the function of the relationship between dose and response and are used to calculate the probability of infection based on the ingested amount of water for a person in each QMRA scenario. The risk assessment is conducted for both the maximum and median values of pathogen to determine whether it is safe to swim in the ocean or not.

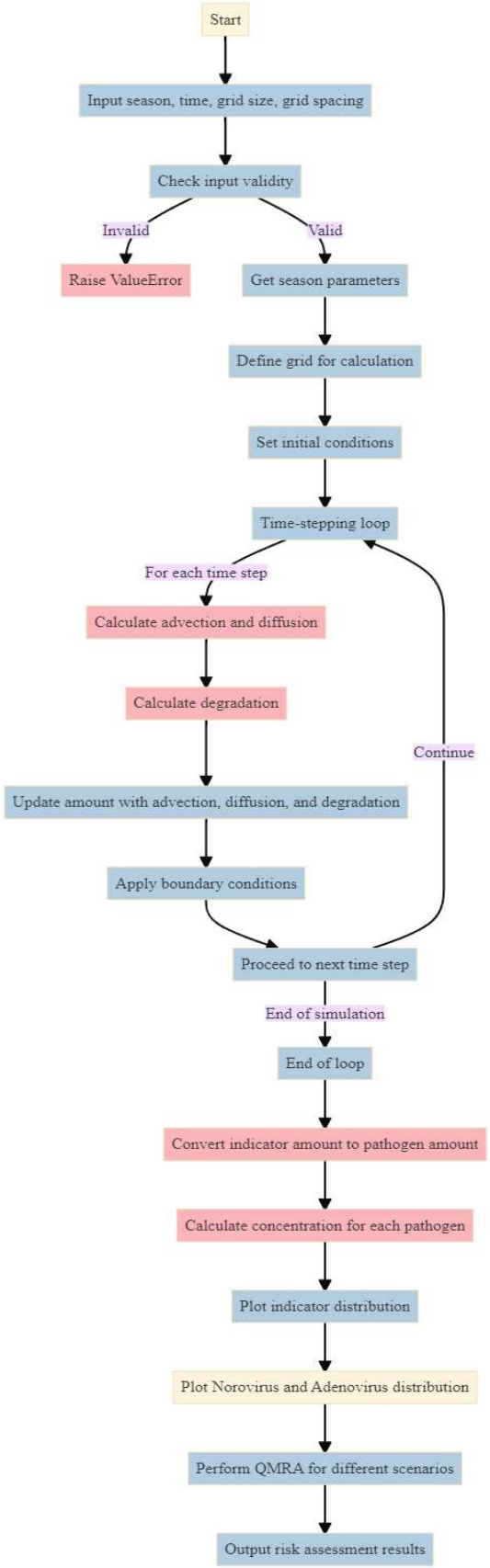

Figure 8: Flow Diagram of the program

3.2. Input Data

3.2.1. Faecal Indicator Bacteria FIB

Faecal contamination of water bodies can lead to outbreaks of waterborne diseases [20], [21]. Since faeces can contain many different pathogens for which testing is expensive and complicated, an alternative method to detect faecal contamination is to test for Faecal Indicator Bacteria instead [1], [2]. According to Sokolova [2] the indicator bacteria should not be pathogens themselves but exist in both human and animal faeces in large amounts. Additionally, they should react similarly to water treatment processes and be easily detectable [2]. Both in drinking and bathing waters coliforms, specifically *E. Coli*, and *Enterococci* are being used as indicators of faecal contamination [20]. Nevertheless, the use of Faecal Indicators also has its downsides. For one there is no consistent relationship between the presence of Faecal Indicator Bacteria, pathogens and a risk to human health [1]. Secondly the presence of FIB by themselves does not necessarily equate to the presence of pathogens as their source cannot be traced back and it does not necessarily be faecal [3].

While most *E. Coli* strains are not pathogenic themselves, their presence is often related to the presence of other pathogenic microorganisms, so it is often used as an indicator for pathogenic contaminations [22]. *E. coli* naturally occurs in the gastrointestinal system of humans and other animals [23]. According to Hussain et al. [24] other than *E. Coli* the group of coliforms is often used as an indicator, since they are part of the human digestive system as well as in animals. Additionally, coliforms are easily detectable, and *Enterococci* are often used as faecal indicators since they can persist in the environment and are usually present in human faeces in amounts of $10^4 – 10^6$ bacteria per gram wet weight. Since *Enterococci* are often used as indicator bacteria there are multiple available detection methods, including standardized methods for its detection in water [24]. Following Korajkic et al. studies have shown less statistically significant correlations between FIB and different pathogens than studies conducted in freshwater, but the significance of the relation increased in waters that had been known to be impacted by faecal contamination. The most correlations between FIB and pathogens have been found to come from *Enterococci*. *Enterococci* also have shown the closest relation to formation the of waterborne illnesses compared to other FIB [3].

Since in previous projects of IMPETUS and iBathwater *E. coli*, *Enterococci* and coliforms have been tracked they are to be used as Indicator Bacteria. The results of iBathwater have shown that Adenovirus has a higher derived risk than Norovirus and Campylobacter [25].

3.2.2. Impacts of environmental conditions on FIB

Due to the availability of data the impacts of environmental conditions on the FIB will be discussed under the assumption that they behave similarly to the associated pathogens. The main factors impacting FIB survival in sea water are temperature, salinity, pH and solar radiation although other factors like competition for nutrients or algae toxins may contribute to it as well. Additionally, the combination of multiple of these effects seems to have an even bigger effect on the bacteria [26].

According to Mancini [27] for the mortality of coliforms from wastewater being diluted in a receiving water three different patterns have been identified by previous studies. The first pattern shows a first order of mortality, the second one an initial increase that is followed by a first order mortality. The third pattern that was discovered began like either of the previous ones but was followed by a reduced mortality rate over time after the overall population had decreased [27].

To calculate the microbial decay, it is assumed to be a first-order process and (1) will be used [23].

$$\frac{dC}{dt} = -k * C \quad (1)$$

When the degradation rate k is constant, this leads to an exponential relationship, which can be seen in (2) [23].

$$C = C_0 * e^{-kt} \quad (2)$$

In this case the degradation rate k is calculated as the sum of the degradation rates for each environmental condition.

Temperature

To predict the effect of temperature on microbiological activity and growth the Q_{10}-Model can be used. The Q_{10} coefficient is the correlation between a change in biological rate and an increase in temperature of 10 °C [28], [29]. Temperatures under 15 °C have shown to either stop *E. coli* growth or even lead to a reduction of the number of *E. coli* present [28].

Other studies have shown that faecal indicator bacteria like *E. coli*, coliforms and intestinal *Enterococci* persist longer in dark, cool environments than in warmer and lighter ones [30]. The temperature of sea water has a big impact on the survival of faecal coliform. The time T_{90}, after which 90 % of coliforms have died off, has been shown to decrease by 55 % for every 10 °C increase in water temperature. This effect is even stronger when the bacteria are also exposed to solar radiation [26].

From data collected from a mixture of wastewater and either fresh or sea water Mancini [27] found the daily mortality rate of coliforms in sea water at 20 °C to be K_{20}=1,4/d (per day). The coliform mortality rate K can be calculated as described in (3) [27].

$$K_{temp} = K_{20} * 1{,}07^{(t-20)} \quad (3)$$

K_{temp}: coliform mortality rate per day at temperature t (°C)

K_{20}: daily mortality rate at 20 °C (1,4/d)

t: temperature in °C

Equation **Fehler! Verweisquelle konnte nicht gefunden werden.** now shows an increase of the degradation rate with an increase in temperature.

Acidity/Alkalinity

The optimal pH for the survival of faecal coliforms in seawater lies between 6 and 7. Outside this range the faecal coliforms degrade rapidly. In the acidic range for each pH value T_{90} decreases by about 40 %, in the alkaline range just by about 30 % per pH value [26]. For *E. coli* on the other hand the optimal pH range was found to be at pH 5, so in acidic conditions. Seawater usually has a pH around 8, which increases the mortality rate of *E. coli* [31]. At the coast of Barcelona, the pH usually varies within a range of 0,15 to 0,2 pH units [32]. Since the variation of the pH is so little and very little data exists for the correlation of pH and FIB degradation, the influence of the pH will not be considered in the calculation of the degradation rate [33].

Salinity

Following research from Solic and Krstulovic [26] faecal coliforms have been shown to have higher inactivation rates at higher salinities, although the effect appeared to be stronger at lower salinities. In the range of 15 – 40 % salinity a 5 % increase led to a decrease of 15 % in T_{90}.

The effect of salinity may either stem from an osmotic effect or from specific ion toxicity. Moreover, higher sunlight exposure also has been shown to increase the inactivation due to salinity, which means both effects may function collectively [26].

A study found decay rates of 0,617/day for *E. coli* and 0,933/day for *Enterococci* in marine waters at 20 °C [29]. Another study researched the inactivation rates of Faecal coliforms based on salinity and temperature. The values in Table 5 have been obtained [34].

Table 5: Bacterial inactivation rates depending on salinity (Data: [34])

	Winter 16 °C	Spring 20 °C	Fall 24 °C	Summer 28 °C	Average
Salinity ‰	k (1/h)	k (1/h)	k (1/h)	k (1/h)	k (1/h)
20	0,0193	0,0252	0,0262	0,0387	0,02735
25	0,0208	0,0274	0,0307	0,0531	0,033
30	0,0215	0,028	0,0441	0,0723	0,041475
35	0,0232	0,0294	0,0649	0,1146	0,058025
40	0,0261	0,0325	0,0838	0,1325	0,068725

Calculating the slope of the linear trendline through the average values for each concentration of salinity leads to a degradation rate of 0,051732/day for Faecal coliforms.

According to Mancini the following equation can be used to calculate the daily mortality rate for coliforms [27].

$$K_{sal} = 0{,}8 + 0{,}006 * (\%\ sea\ water) \quad (4)$$

Since in this case a mixture of fresh and sea water was used, so a salinity of 35 ‰ would be shown as 100% in the equation (97,14 % of seawater equals 34 ‰) [27], [35]. With this information **Fehler! Verweisquelle konnte nicht gefunden werden.** can be adjusted for the simulation as follows:

$$K_{sal} = 0{,}8 + 0{,}006 * (\frac{salinity}{3{,}5} * 100) \quad (5)$$

UV Radiation/light

Studies have shown that being exposed to sunlight leads to up to 10 times greater inactivation rates in faecal indicators like faecal coliforms and *Enterococci* in seawater [36]. It can damage the cellular components or cause photooxidative damage [20]. According to Solic and Krstulovic solar radiation appears to have a bigger impact on the degradation of faecal coliforms than the temperature as well as enhance the impact of temperature. An increase in solar radiation by 100 W/m^2 decreases T_{90} of faecal coliforms by about 40 %. Depending on UV intensity 90 % of faecal coliforms died off between approximately one and five hours, while in the dark it took between 51 to 145 hours [26]. For *Enterococci* the decay rates from sunlight lie between 0.1 and 6 h^{-1}, while the decay rate in the dark is between 0,005 and 0,03 h^{-1} [20]. Additionally, the presence of sunlight enhances the effects of temperature and salinity on faecal coliforms [26], [36].

Another study compared the decay rates of *E. coli* and coliform bacteria under light and dark conditions, both at 15 °C. The decay rates for *E. coli* were 0,33/day in the dark and 0,65/day under light conditions, and for coliforms 0,3/day in the dark and 0,26/day in light. [30]

To calculate the degradation based on UV radiation (6) is to be used [35].

$$k = k_l * I \quad (6)$$

k_l was determined to be 0,32 cm^2/cal while I is the solar radiation in Ly/hour (1 Langley = 1 cal/cm^2) [35]. Following (6) the degradation factor coming by UV radiation is set to be 0 at night, since there is not radiation (I).

Since CSO happen during heavy rainfalls it is likely cloudy during and at least for a few hours after the event, which reduces the pathogen degradation rate.

3.2.3. Pathogen concentrations at Bogatell beach

The Barcelona Public Health Agency (Agència de Salut Pública de Barcelona ASPB) monitored the water health of the beaches in 2017 based on samples taken from April to September. Samples were usually collected on Mondays between 9 and 11 am and analysed for internal *Enterococci* and *E. coli*, which functioned as Faecal Indicator Bacteria FIB (3.2.1 Faecal Indicator Bacteria FIB). The samples were taken 30 cm below the surface at points with at least 1 m depth.

The average results for Bogatell beach for the swimming season of 2016 showed a concentration of intestinal *Enterococci* of 137 CFU/100 ml in the 90th percentile and 866 CFU/100 ml in the 95th percentile. *E. coli* was detected with a concentration of 194 CFU/100 ml in the 90th percentile and 527 CFU/100 ml in the 95th percentile. Based on these values the sanitary quality was classified as sufficient. ASPB also found a close relationship between the sanitary quality of the beaches and the rainfall tracked at the Barcelona-Raval station, located approximately 3 km from Bogatell beach. According to the study the increased levels of FIB concentration stem from discharges of untreated wastewater into the ocean and usually have a short-term impact of less than 72 hours.

From April to May 2017 weekly samples were taken from various beaches in Barcelona by the ASPB, including Bogatell while from June to September the frequency was reduced to twice a month. Usually, the quality was classified as excellent and once as good, with the only exception being on the 24th of July, where it was deemed insufficient, not only in Bogatell but in 9 out of 10 beaches overall. On the previous day, the 23rd of July 2,8 mm of rainfall were recorded [37]. This relation between rainfall and a decrease in the sanitary quality of beaches has been found in other beaches in Barcelona as well [38]. There is no data available to know if a CSO occurred during the rainfall on the 23rd of July, but the increase of FIB makes it a possibility.

Following the decreased water quality on the 24th an additional sample was taken on the 26th of July, which also showed increased numbers of FIB, likely due to another rain event on the 25th of July [38].

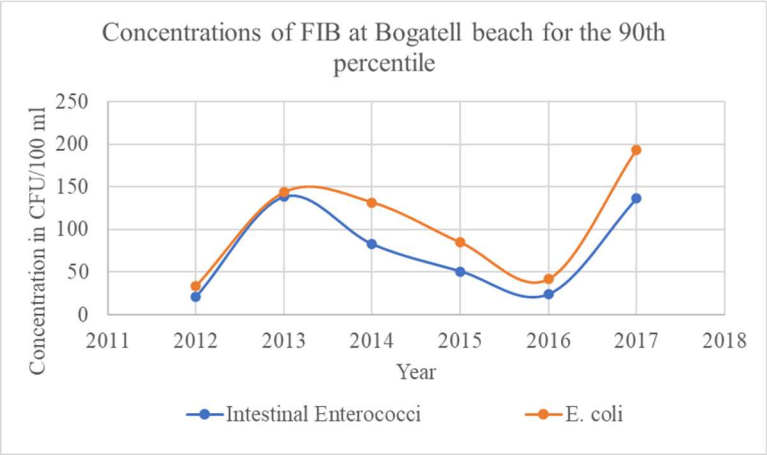

Figure 9: Concentrations of Intestinal *Enterococci* and *E. Coli* at Bogatell beach for the 90th percentile (Data from ASPB: [38])

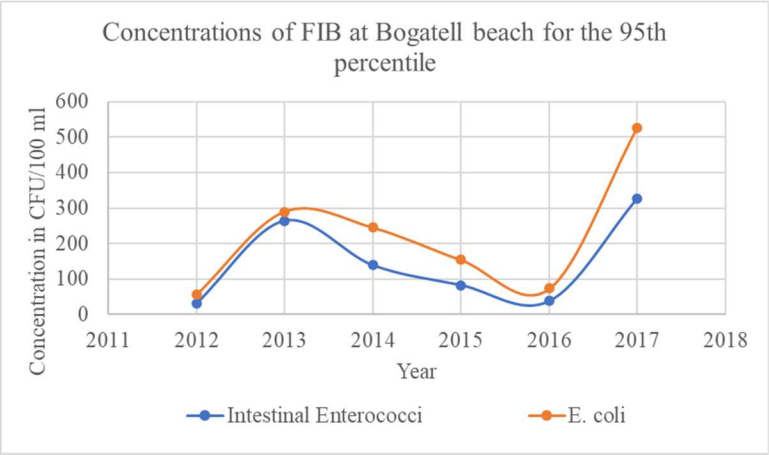

Figure 10: Concentrations of Intestinal *Enterococci* and *E. Coli* at Bogatell beach for the 95th percentile (Data from ASPB: [38])

Figure 9 and Figure 10 show the concentrations of Intestinal *Enterococci* and *E. Coli* at Bogatell beach for the years 2012 to 2017 as detected during the study of the Barcelona Public Health Agency ASPB. The data for both the 90th and 95th percentile shows the strongest increase of FIB from 2016 to 2017. The same study labelled the sanitary quality of Bogatell beach excellent in 2012, 2015 and 2016, good in 2014 and sufficient in 2013 and 2017. The increase of FIB concentrations is attributed to the meteorological episodes during July and September 2017, which has affected other beaches in Barcelona as well [38].

3.2.4. Previous CSO Data

In 2024 data has been collected during and after three CSO events in Bogatell beach, on the 10th of January, the 22nd of April and on the 29th of April. These are three short-term episodes of overflow of untreated water [39]. The precipitation measured at the airport in Barcelona on the 10th of January was 2,8 mm, 10,2 mm on the 22nd of April and 68,4 mm on the 29th of April [37]. The airport is located approximately 15 km southwest of Bogatell beach.

Figure 11 shows the volume of wastewater that was released during the CSO in January, a total of 15860,7 m^3. Most of the volume was released within about three hours, between 17:30 and 20:30 on the 10th of January.

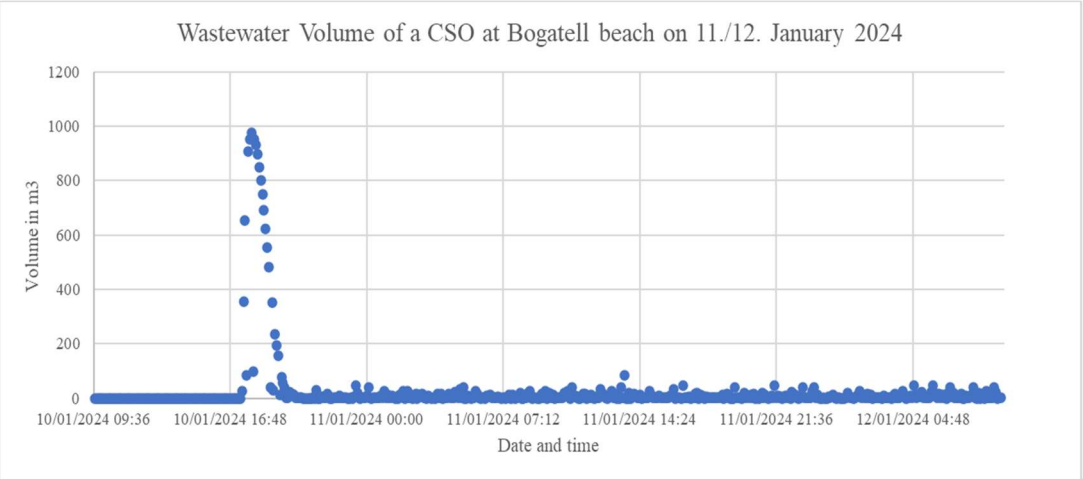

Figure 11: Wastewater volume released at Bogatell beach during the 11th and 12th of January 2024 (Data: [39])

Figure 12 shows the released volume during the first CSO in April, which was a total amount of 137355,6 m^3. Most of the water was released 16:30 and 22:30 on the 22nd of April, so during approximately 6 hours.

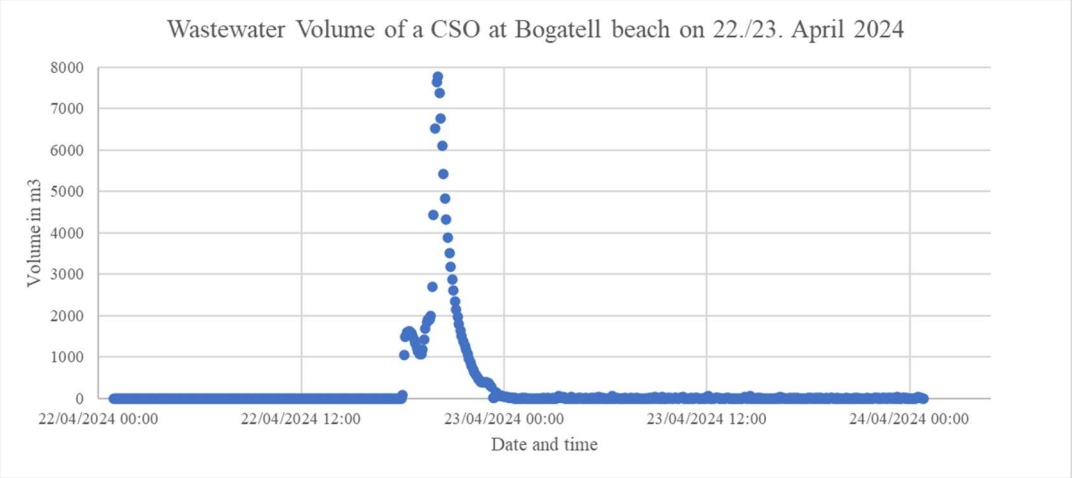

Figure 12: Wastewater volume released at Bogatell beach during the 22nd and 23rd of April 2024 (Data:[39])

The second CSO in April is displayed in Figure 13, during this event a total of 331158 m^3 was released into the sea. This CSO is basically a combination of two events, the first one lasting from 03:10 on the 29nd of April until 09:30 and the second one happened between 11:10 on the same day and ended at 02:30 on the 30th of April.

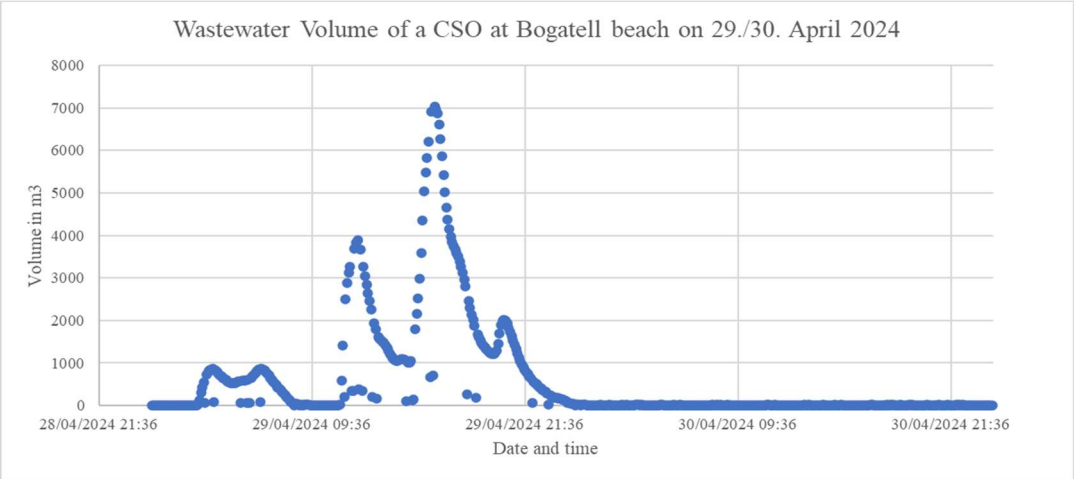

Figure 13: Wastewater volume released at Bogatell beach during the 29th and 30th of April 2024

Within the IMPETUS project water samples have been taken at Bogatell beach during and after these three CSO events. For each one 20 litres of water have been taken at the starting point inside the breakwater, the first one three hours after the start of the CSO and the next one 24 hours later. The samples were analysed for human Adenovirus HAdV and Norovirus Genogroup I and II (NoV GI and NoV GII). Additionally, all samples in April were also tested for *E. coli* and intestinal *Enterococci* as FIB and measured in Most Probable Number MPN/100ml. The concentrations of viruses and FIB were measured in genomic copies per litre (GC/l) [40].

Table 6: Results of Sea Water Analysis from January 11th and 12th 2024 (Data: [40])

	Human Adenovirus (HAdV)	Norovirus Genogroup I (NoV GI)	Norovirus Genogroup II (NoV GII)
	GC/l	GC/l	GC/l
11.01.2024	198	6130	13300
12.01.2024	37,3	4320	3040

The results from the CSO in January are shown in Table 6. The analysis of the samples from January show that after 24 hours the pathogens are still present in the water, although in lower concentrations, which may be a result of both degradation and dilution in the sea water, as well as distribution to other areas.

Table 7: Results of Sea Water Analysis from April 22nd and 23rd 2024 (Data: [40])

	Human Adenovirus (HAdV)	Norovirus Genogroup I (NoV GI)	Norovirus Genogroup II (NoV GII)	*E. coli*	Intestinal *Enterococci*
	GC/l	GC/l	GC/l	MPN/100 ml	MPN/100ml
22.04.2024	6000	37900	1840	2250	3550
23.04.2024	1020	1900	317	2390	3180

The first two samples taken in April are displayed in Table 7 and show a reduction of the number of pathogens within 24 hours as well as the number of *Enterococci*, although there is a slight increase in the number of *E. coli* that was detected.

Table 8: Results of Sea Water Analysis from April 29th and 30th 2024 (Data: [40])

	Human Adenovirus (HAdV)	Norovirus Genogroup I (NoV GI)	Norovirus Genogroup II (NoV GII)	*E. coli*	Intestinal *Enterococci*
	GC/l	GC/l	GC/l	MPN/100 ml	MPN/100ml
29.04.2024	23400	33400	2700	43300	1850
30.04.2024	4860	3310	178	967	311

The results of the third CSO are shown in Table 8. Between the last two samples taken in April another overflow happened in this location, which is also visible in Figure 13, but still a reduction in the concentration of viruses and FIB was detected.

To assume an initial amount of FIB that is released during the CSO event the data from the CSOs in April 2024 will be used, since during the CSO in January the concentration of FIB was not measured. During the first event a total of 137355,6 m^3 was released and 331158 m^3 during the second event. Based on the measurements of FIB (*E. coli* and *Enterococci)* taken during the first CSO event in sum a total of 5800 MPN/100ml was released and 45150 MPN/100ml during the second CSO event. Multiplying these concentrations with the respective wastewater volumes leads to a total amount of FIB of 7.97E+12 in the first and 1.495E+14 in the second case. For the simulation the largest amount will be assumed to calculate the worst-case scenario.

3.2.5. FIB to pathogen ratios

With the available data from the samples taken in April 2024 new ratios between FIB and pathogens in the water can be calculated. For simplicity the values for both groups of Norovirus have been summed up together before the ratio has been calculated.

Table 9: Pathogen to Indicator Ratios from IMPETUS data in 2024 (based on Data from [40])

	AdV : *E. coli*	AdV : *Enterococci*	NoV : E.coli	NoV : *Enterococci*
22.04.	0,26667	0,16901	1,76622	1,11944
23.04.	0,04268	0,03208	0,09276	0,06972
29.04.	0,05404	1,26486	0,08337	1,95135
30.04.	0,50259	1,56270	0,36070	1,12154
average	0,21649	0,75716	0,57576	1,06551

Table 9 shows the average values for the ratios between the pathogens Adenovirus and Norovirus in relation to *E. Coli* and *Enterococci* as Indicator bacteria.

Previous research from the iBathwater project has determined the pathogen to indicator ratios displayed in Table 10. They are based on samples taken during 2020 and 2021 at Bogatell Beach. The ratios have been calculated for Norovirus and Adenovirus with *E. Coli* and *Enterococci* as indicators.

Table 10: Pathogen to Indicator Ratios from iBathwater from 2020/2021 (Data: [41])

AdV : *E. Coli*	AdV : *Enterococci*	NoV : *E. Coli*	NoV : *Enterococci*
0,00448	0,00813	0,00166	0,0026

A study conducted in Norway in 2016 also examined the relationship between *E. Coli* and different pathogens in seawater after CSO events. It found a ratio between Norovirus to *E. coli* of 0,0864 [11].
In order to assume the worst-case scenario, the highest ratio of pathogen to FIB will be used, which in this case is the Norovirus to *Enterococci* ratio from the IMPETUS data (1,06551:1) and the Adenovirus to *Enterococci* ratio (0,75716:1) from the IMPETUS data as well.

3.3. Simulation in Python

To simulate the pathogen distribution in water a set of equations have to be solved at discrete time steps on a grid covering the area [42]. In this case Python will be used for the simulation and to run the model.

Python is a free, open-source programming language which aims to use an expressive syntax that results in a code which is easy to read [43].

3.3.1. Assumptions and boundary conditions

In order to simulate the distribution of pathogens using Python some simplifications and assumptions of the real-world scenario had to be made. First of all, the distribution is to be calculated only in x- and y-direction as a 2D-model, so the water depth will not be taken into account.

Secondly four scenarios will be used, one for each season, with average values for environmental conditions such as temperature or speed and direction of the ocean currents. The weather data is used as previously described and the data on speed and directions of the currents from COSMO [18].

To include speed and direction of the currents in the simulation the velocities from Table 4 must be separated into x- and y-direction using trigonometry and the angle relative to the beach. The total velocity is assumed to be the hypothenuse of a right triangle, with x as the opposite and y as the adjacent side. The angle is determined by the direction out of which the current is coming according to COSMOS.

$$velocity_x = \frac{\sin(\alpha)}{velocity_{total}} \tag{7}$$

$$velocity_y = \frac{\cos(\alpha)}{velocity_{total}} \tag{8}$$

Only in February and June the sea currents go into the direction of Bogatell beach, since they are coming from the South-East, which is the direction the beach faces. Since these are the worst conditions and the pathogens are most likely to be transported into the direction of the beach, these are the values that will be used in the simulation for winter and summer. For spring and autumn, the average values of the respective months will be used. The results are displayed in Table 11.

Table 11: Velocities used for each season

	Winter	Spring	Summer	Autumn
x-velocity (m/s)	-0,01	0,03	-0,01	-0,04
y-velocity (m/s)	-0,01	0,00	-0,01	0,00

The model includes the beaches on both sides of the CSO source point, approximately 605 m to the west and 480 m to the east. This area is covered by a grid for which the size can be set in the program, which basically defines the resolution. In this case a grid size of 100 was used, meaning there are one hundred grid points in each dimension. A higher grid size increases accuracy while also leading to longer computation times.

The actual position of the point source of the CSO is between two concrete barriers of the breakwater, which are approximately 75 m apart and extend about 170 m into the ocean. Since neither pathogens nor water can pass through these barriers all the untreated water can only go in one direction into the ocean. So, for simplicity in the simulation the point source is located right at the other end of the breakwater, which is the most conservative estimation, as in reality the complete volume of the untreated water from the CSO would not reach the ocean at the same time, but rather spread over a period of time and already more diluted.

3.3.2. Equations

The basis of the simulation is formed by the general transport equation or advection-diffusion dispersion equation, which combines the effects of advection, diffusion, and pathogen degradation [42]. Transport by advection happens through the movement of the sea currents while diffusive transport happens through turbulent mixing. Diffusion increases the size of the contaminated area although the concentration of pathogens is becoming more diluted [42].

For a scalar quantity like a concentration in a fluid is it displayed as follows:

$$\frac{\partial C}{\partial t} + \nabla(vC) = D\nabla^2 C - \lambda C \tag{9}$$

C: concentration of the scalar quantity
v: velocity field (with components v_x and v_y)
D: diffusion coefficient
λ: degradation rate (depending on environmental factors)
∇*(vC): advection
$D\nabla^2C$: diffusion
-λC: degradation

From (9) the following equation can be derived for the change of pathogen concentration [44]:

$$\frac{\partial C}{\partial t} = -v * \nabla C + D\nabla^2 C - kC \tag{10}$$

Each part of this equation will be described in more detail in the following chapters. To calculate the pathogen distribution and degradation the terms from the general transport equation will be discretized.

3.3.3. Advection

Firstly, to calculate the velocity in both x- and y-direction two equations are necessary for each, in order to include both positive and negative directions in Python. For each grid point the change in concentration due to water flow in x- and y-direction is calculated.

$$advection_x = v_x \frac{C(i,j)-C(i,j-1)}{\Delta x} \quad (11)$$

$$advection_x = v_x \frac{C(i,j+1)-C(i,j)}{\Delta x} \quad (12)$$

$$advection_y = v_y \frac{C(i,j)-C(i-1,j)}{\Delta y} \quad (13)$$

$$advection_y = v_y \frac{C(i+1,j)-C(i,j)}{\Delta y} \quad (14)$$

C(i,j): Pathogen concentration at grid point (i,j)
v_x, v_y: Velocity components in x- and y-direction

3.3.4. Diffusion

To include the spreading of pathogens due to diffusion the Laplacian of the concentration field for neighbouring grid points is calculated using the following equation [45].

$$laplacian = C(i+1,j) + C(i-1,j) + C(i,j+1) + C(i,j-1) - 4C(i,j) \quad (15)$$

The Laplacian calculates the concentration change at each point based on its neighbours.
Then the diffusion term can be calculated using [45]:

$$diffusion = D \frac{laplacian}{(\Delta x)^2} \quad (16)$$

D: Diffusion coefficient
Δx: grid spacing
For the diffusion coefficient of water 10^{-5} will be used [46].

3.3.5. Degradation

Using k_{pH}, $k_{temperature}$ and $k_{uv\_intensity}$ as degradation rates for temperature, salinity, and UV radiation this can be adapted to the simulation to reduce the concentration according to the current environmental conditions. The degradation rates for each environmental factor have been described in chapter 3.2.2.

$$degradation = \left(k_{Salinity} + k_{temperature} + k_{uv_{intensity}}\right) * C * dt \quad (17)$$

dt: time step size

3.4. Quantitative Microbial Risk Assessment (QMRA)

The health risks of recreational use of surface waters have been shown to increase with higher amounts of present FIB when they originated from human faeces [1]. Outbreaks of waterborne diseases from the recreational use of water bodies are usually related to pathogenic microorganisms [3].

QMRA is used to estimate the risk of an infection or illness to the exposure of microorganisms based on the relation of dose and response, so the number of pathogens related to their effects on human health [47]. It takes into account the presence, transport and potential degradation of the pathogens as well as the possible exposure scenarios for humans and the possibly resulting health effects [48].

According to the WHO the QMRA is conducted in four steps, starting with the hazard identification and context definition, which includes the reference pathogens, exposure pathways and possible health effects. The next step is the exposure assessment in which the magnitude and frequency of exposure along the defined exposure pathways are quantified. It is followed by the health effects assessment, in which the exposure dose of pathogens is linked to

the infection probability. Lastly during the risk characterisation, the collected information is combined to quantify the risk [48].

While the QMRA is an evidence-based risk assessment method that provides a detailed quantification, it is still dependent on the data availability of pathogen detection. For lacking data assumptions have to be made, which are generally more conservative, so that the risk for the worst-case scenario is assessed. This may lead to an overestimation of the actual risk [48], so in this case this may lead to people being warned against swimming at Bogatell beach.

3.4.1. Hazard identification

The objective of this QMRA is to assess the risk posed by pathogens in the seawater after a CSO event to beachgoers. The FIB considered are intestinal *Enterococci*, *E. coli* and coliforms, which are being related to Norovirus and Adenovirus, since these are the only pathogens and related FIB for which data is available from the IMPETUS project. In reality there are various other pathogens contained in wastewater, but due to the availability of data these will be the ones focused on in this assessment.

According to Haas et al. Noroviruses are one of the major causes of viral gastrointestinal diseases in the world. They have an incubation period of 1 – 2 days and the resulting illness usually lasts 1 – 2 days as well. The most common symptoms are nausea, abdominal cramps and vomiting or diarrhoea. There is no lasting protection against Noroviruses and reinfections are possible. The disease can be deadly, although this mostly effects elderly or immunocompromised people [23].

Adenoviruses on the other hand can cause various different illnesses, they cannot only affect the digestive system, but also cause eye or respiratory infections. They have an incubation period of 8-10 days, and the symptoms usually persist for 8 days. Adenoviruses have a higher mortality rate than noroviruses and in immunocompromised people rates of up to 50 – 60 % have been reported [23].

3.4.2. Exposure assessment

Different exposure scenarios have to be assessed, as depending on duration and activity the amount of ingested water can vary. In IMPETUS three different scenarios have been considered, low (rowing, boating, fishing, non-capsizing kayaking and canoeing, etc.), middle (kayaking and capsizing with occasional capsizing) and high (swimmers) volumes of ingested water [25].

Unintentional ingestion during recreational swimming has the highest ingestion rate [48]. The amount of ingested pathogen depends on their concentration in the water and the ingested volume [11]. For the ingested volume there are different values available in literature, for this scenario the assumption is that an adult ingests 16 ml of water per hour of swimming and a child 37 ml [11], [23], [49]. Aside from the faecal-oral route infections through the respiratory system or the eyes are also possible [23]. For activities on the water, it will be assumed that 2 ml of water will be inhaled per hour [50].

Table 12: Risk Assessment Scenarios

	Scenario	Exposure pathway	Ingested amount of water
A	Child swimming	Swallowing	37 ml per hour
B	Adult swimming	Swallowing	16 ml per hour
C	Activity on water	Inhalation	2 ml per hour

In this case the pathogens come from the mix of waste- and rainwater released into the sea during the CSO event. Their persistence in the ocean depends on various factors, which have previously been discussed. Since CSOs happen infrequently the assessment is conducted for a single exposure. For the risk assessment one hour will be assumed for the duration of recreational activity on the beach.

3.4.3. Dose-Response Model

According to Eregno et al. the dose-response model associates the risk of infection to the dose of a pathogen a person is exposed to. An infection means that a microorganism can grow or multiply within a host but does not necessarily lead to the outbreak of an illness, as this depends on different factors such as the virulence of the pathogen, the health and immune status of the person and the amount of ingested pathogen [11], [23]. Enteric infections lead to diseases in about 50 % of the cases [23]. While in theory even one singular bacterium or virus could be enough to infect a person, due to the reaction of the immune system this is unlikely to occur. The actual dose to cause an infection may vary for each person, depending on factors like their age, health etc. Generally exponential or beta models are used to determine the necessary threshold [23]. The models were chosen based on the availability of data on the dose-response parameters.

Following the study conducted by Eregno et al. in Norway for Norovirus the beta-Poisson model is applied. In (18) p is the probability of infection and d the ingested dose [11].

$$p = 1 - (1 + \frac{d}{\beta})^{-\alpha} \tag{18}$$

$$ID_{50} = \beta * (2^{\frac{1}{\alpha}} - 1) \tag{19}$$

The parameters needed for the beta-Poisson curve in (18) and the average dose for infection ID_{50} in (19) are defined as $\alpha = 0{,}04$ and $\beta = 0{,}055$ [11].

To calculate the probability of an Adenovirus infection the exponential model will be used, as shown in (20) [51], [52].

$$P = 1 - e^{-k*d} \tag{20}$$

According to research from the Michigan State University the parameters are defined as k=6,07E-1 and ID_{50}=1,14 [51].

3.4.4. Risk Characterisation

The risk of infection will be calculated for both children and adults per single exposure by swimming at the beach during the days following a CSO events, as well as for a person doing a recreational activity on the water (kayaking, rowing etc.).

In order to assess the risk in the worst-case scenario the highest number of FIB and the associated amount of pathogen will be used for the assessment and compared to the average values for a more realistic scenario.

According to the United States Environmental Protection Agency USEPA the US, EU and WHO usually use a risk threshold of 1 – 2 % for gastrointestinal illnesses from the use of recreational waters [53]. For this assessment the risk threshold of 2 % will be used.

3.4.5. Risk Assessment in Python

Since in the simulation the distribution of the total amount of pathogen was modelled and the depth of the water was not considered some assumptions have to be made to conduct the risk assessment, especially to calculate the ingested dose of pathogens. Since the grid size and associated pathogen amount are known, a water depth of one meter will be assumed to estimate the volume in which the pathogens are contained. This is not an entirely accurate estimation, but the pathogen spread over depth has not been considered in the simulation. Also, since for

most parts of the area the depth is likely larger than one meter, the pathogens would be even more diluted, so this is a rather conservative approach.

Firstly, in order to assess the risk for the worst-case scenario, the highest present pathogen concentration will be used for the risk assessment and be compared to the average pathogen concentration. Equation (21) is used to calculate the pathogen amount ingested by a person swimming.

$$dose = \mathrm{C} * (\frac{ingestion\ rate\ in\ ml}{1000}) \quad (21)$$

The probabilities of infection are calculated for Norovirus and Adenovirus using the equations and associated parameters displayed in chapter 3.4.3.

4. RESULTS AND DISCUSSION

Using the simulation in Python the distribution and degradation of FIB was simulated for each season. The results show the total amount of FIB, since the depth was not considered in the simulation a concentration could not be calculated. Following the established pathogen to indicator ratios the risk assessment for the previously determined scenarios was conducted.

4.1. Comparison of different scenarios

The FIB distribution after a CSO event varies greatly depending on the season due to the different speed and direction of the sea currents.

Figure 14 shows the FIB distribution one and twelve hours after a CSO event in spring. Due to the direction of the currents coming from NE the contamination is transported from the top of the breakwater parallel to the beach until it leaves the simulated area.

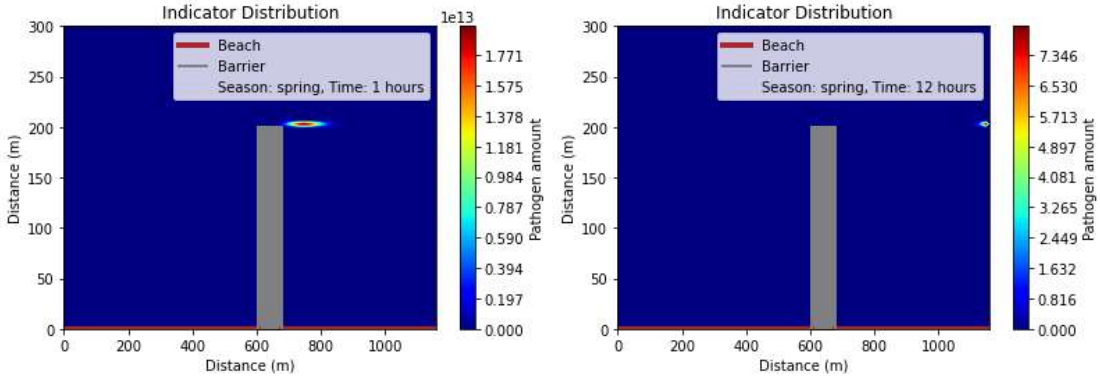

Figure 14: Distribution of FIB after 1 and 12 hours in Spring

In summer on the other hand the currents coming from the south move more into the direction of the beach, which can be seen in Figure 15.

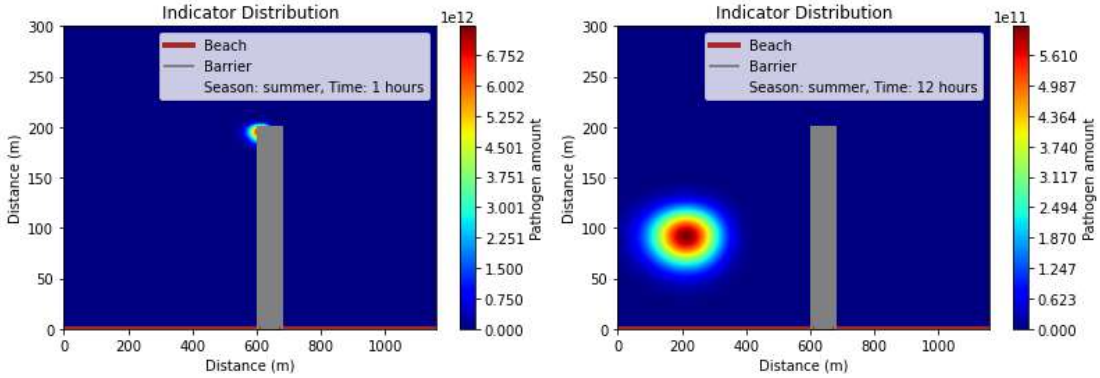

Figure 15: Distribution of FIB after 1 and 12 hours in Summer

Figure 16 shows the FIB distribution in autumn, similar to the spring scenario the contamination is transported parallel to the beach until it leaves the simulated area, but in this case coming from SE.

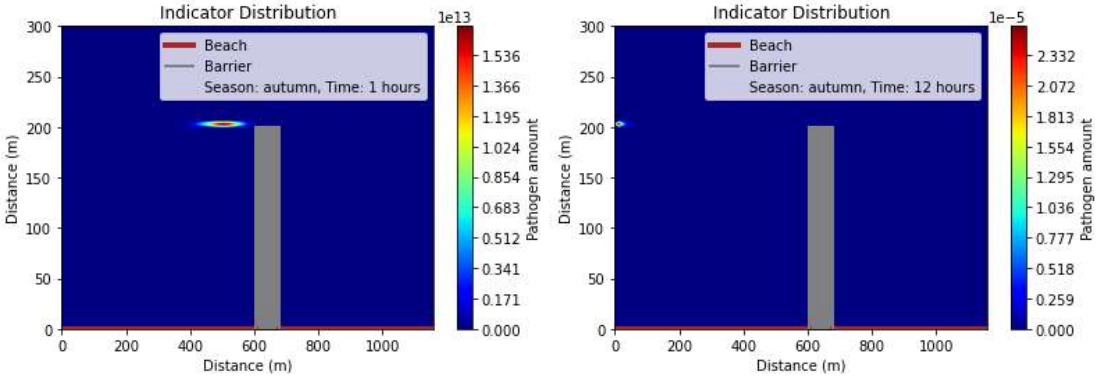

Figure 16: Distribution of FIB after 1 and 12 hours in Autumn

Since in winter the current speed and direction is the same as in summer and comes from the south the output displayed in Figure 17 is almost the same, with minor differences in the overall amount of FIB.

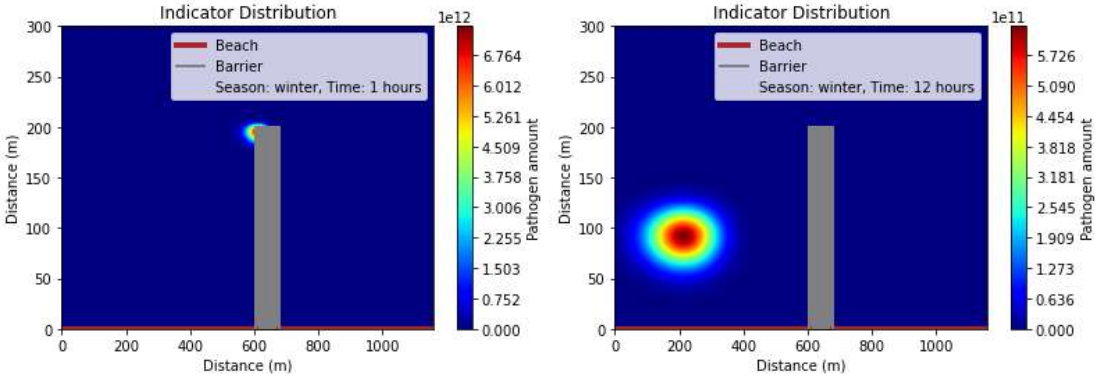

Figure 17: Distribution of FIB after 1 and 12 hours in Winter

The speed and direction of the sea currents have a visible impact on how the contamination is distributed through the sea. Since in summer and winter they are pointing into the direction of the beach the pathogens can get flushed onto the beach, increasing the risk of infection for beach goers.

4.2. Risk assessment

Using the established ratios of pathogens and FIB the amounts of Norovirus and Adenovirus can be calculated for the risk assessment. There are three different scenarios which will be considered in the risk assessment, a child swimming (scenario C), an adult swimming (scenario A) and a person performing secondary activities on the water, like kayaking or rowing (scenario S). The risk is calculated based on the ingested amount of water in one hour associated with each activity as discussed in previous chapters. For a comparison the risk assessment is conducted using both the maximum and average amounts of pathogen for both Norovirus and Adenovirus, so the most conservative worst-case scenario is to be compared to a more realistic one. The risk assessment is conducted for the complete area of the simulation, since it can not be foreseen how far people might swim out into the sea.

4.2.1. Maximum values

The probability of infection for each scenario for 1, 12, 36 and 48 hours after the CSO event using the maximum amounts are displayed in Table 13 and Table 14. The highest risk for Norovirus is observed one hour after the CSO, with probabilities in the range of 65 – 70 %

depending on the scenario, while the risk for an Adenovirus infection starts off at 100 % in each scenario.

Table 13: Probability of Infection for Spring and Summer using the maximum values

		Spring			Summer		
Time	Virus	C	A	S	C	A	S
1h	Noro	0,7021	0,6919	0,6652	0,6904	0,6798	0,6520
	Adeno	1	1	1	1	1	1
12h	Noro	0,0739	0,0491	0,0109	0,6580	0,6463	0,6156
	Adeno	0,1290	0,0580	0,0074	1	1	1
24h	Noro	0	0	0	0,5965	0,5827	0,5466
	Adeno	0	0	0	1	1	1
36h	Noro	0	0	0	0,0016	0,0007	0,001
	Adeno	0	0	0	0,0010	0,0004	0,001
48h	Noro	0	0	0	0	0	0
	Adeno	0	0	0	0	0	0

Table 14: Probability of Infection for Autumn and Winter using the maximum values

		Autumn			Winter		
Time	Virus	C	A	S	C	A	S
1h	Noro	0,7004	0,6902	0,6633	0,6904	0,6798	0,6520
	Adeno	1	1	1	1	1	1
12h	Noro	0	0	0	0,6582	0,6466	0,6159
	Adeno	0	0	0	1	1	1
24h	Noro	0	0	0	0,5972	0,5834	0,5473
	Adeno	0	0	0	1	1	1
36h	Noro	0	0	0	0,0017	0,0007	0,0001
	Adeno	0	0	0	0,0010	0,0004	0,0001
48h	Noro	0	0	0	0	0	0
	Adeno	0	0	0	0	0	0

In spring and autumn, the risk of infection after 12 hours has already gone down to zero, while in summer and spring even after 24 hours there is still a probability of infection of almost 60 %. This encompasses the whole area, especially during the first few hours the pathogens have not reached the beach yet and are mostly spread around the area of the breakwater. At this point swimming close to the beach could still be considered safe.

Figure 18 shows the risk of a Norovirus infection following a CSO event in spring over time. The probability for a child to get an infection is highest since they ingest the highest amount of water. The probability reduces gradually over time and after 12 hours the risk has fallen under 10 %.

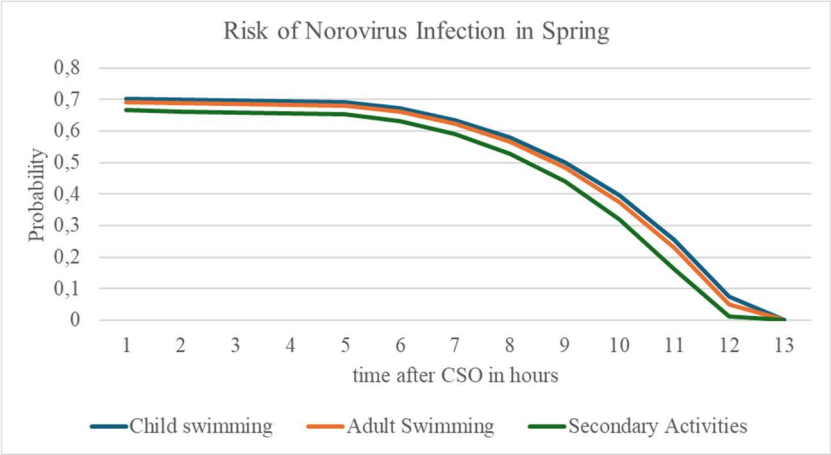

Figure 18: Risk of Norovirus Infection in Spring using the maximum values

In Figure 19 shows the same scenarios for summer. The probability of infection continues for a much longer time, the risk becomes zero about 36 hours after the CSO event, it persists approximately three times as long as in spring.

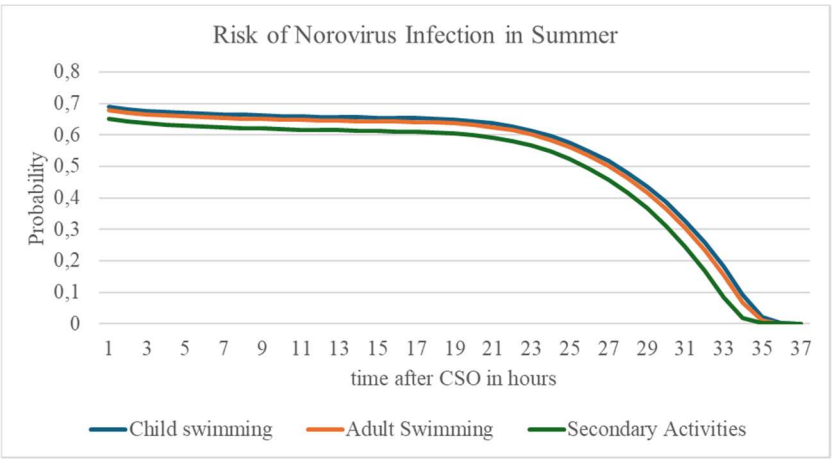

Figure 19: Risk of Norovirus Infection in Summer using the maximum values

In autumn the risk of infection consists for the shortest overall amount, after about 11 hours the probability has become zero, as is shown in Figure 20.

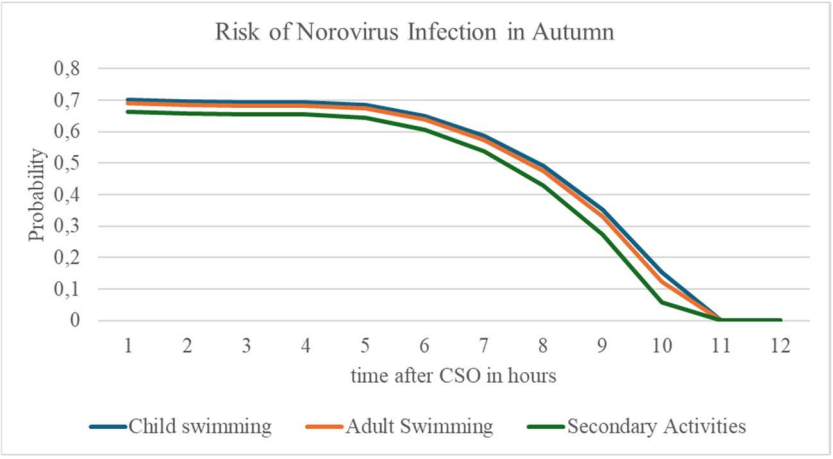

Figure 20: Risk of Norovirus Infection in Autumn using the maximum values

The graph for the winter scenarios runs similarly to the one in summer, it also takes about 36 hours for the probability of infection of Norovirus to be reduced to zero, as shown in Figure 21.

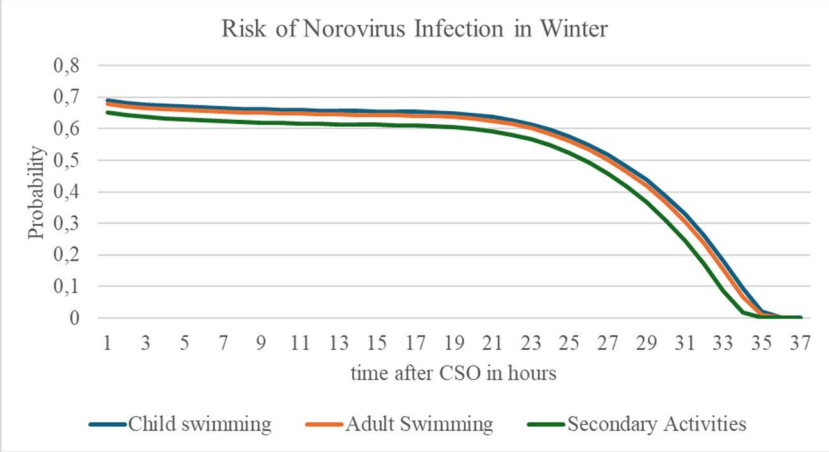

Figure 21: Risk of Norovirus Infection in Winter using the maximum values

Figure 22 shows a comparison the probability of a Norovirus infection for children during each season. The curves for Winter and Summer have the exact same course since in these cases the current speed and direction were the same, only the environmental conditions varied.

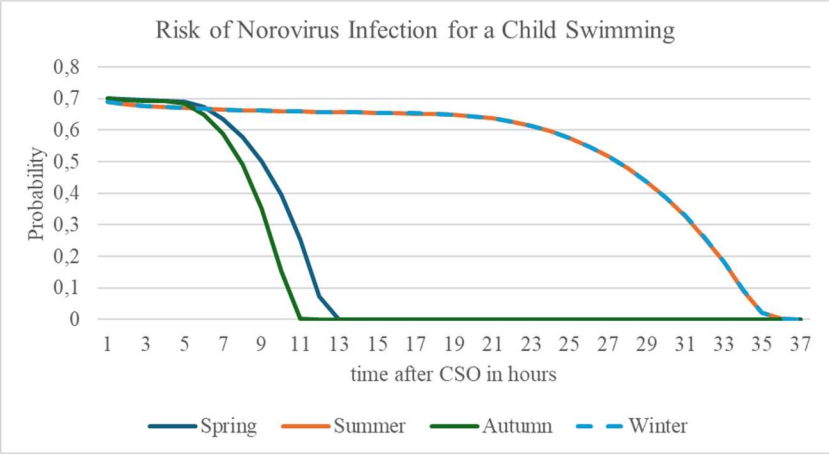

Figure 22: Risk of Norovirus Infection for a child swimming using the maximum values

The same is shown in Figure 23 and Figure 24 for the risks for an adult swimming and performing secondary activities on the water. The shortest time until the probability of infection is reduced to zero happens during autumn, followed by spring.

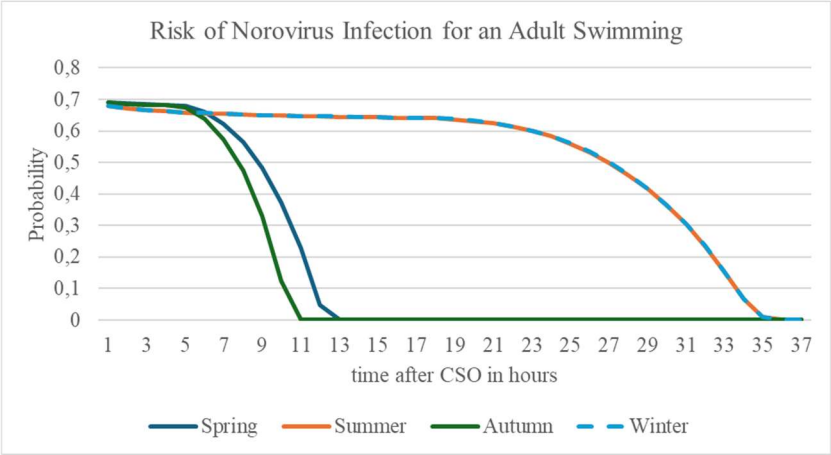

Figure 23: Risk of Norovirus Infection for an adult swimming using the maximum values

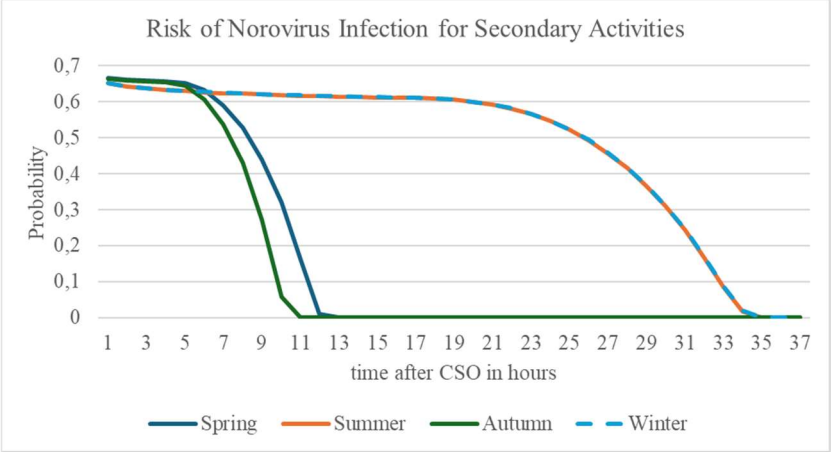

Figure 24: Risk of Norovirus Infection for secondary activities using the maximum values

The same assessment has been conducted for the risk posed by Adenovirus in the water. Figure 25 shows the results for spring. It can be seen that eleven hours after the CSO event there is a steep drop from a 100 % risk of infection to zero after 12 to 13 hours. Due to the direction of the sea currents in spring this happens because at this point the released plume of wastewater leaves the area of the simulation.

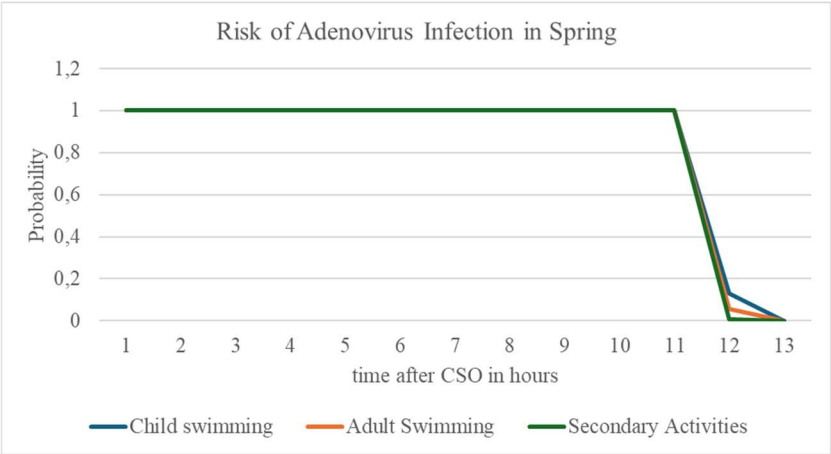

Figure 25: Risk of Adenovirus Infection in Spring using the maximum values

The same happens during summer, which is shown in Figure 26, although it takes longer and in this case the contamination is transported into the direction of the beach. So, the risk might not actually be zero, depending on how the pathogens persist outside the water.

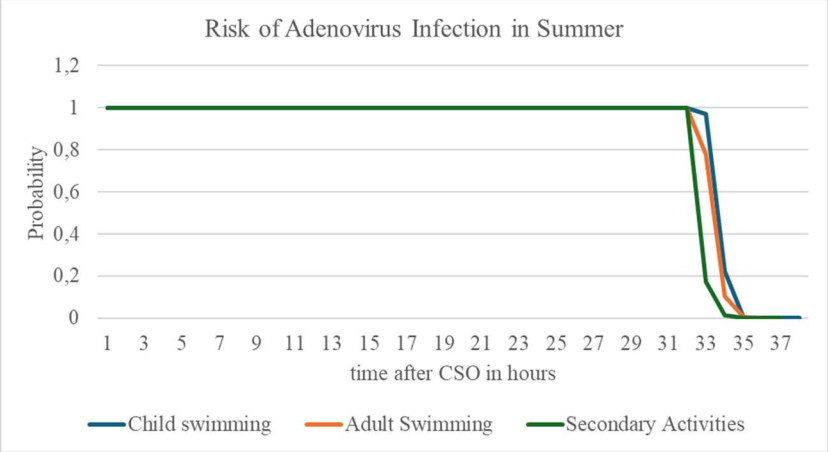

Figure 26: Risk of Adenovirus Infection in Summer using the maximum values

Figure 27 shows the risk of an Adenovirus in autumn. The graph shows the same course as before, after about 9 hours the probability drops steeply.

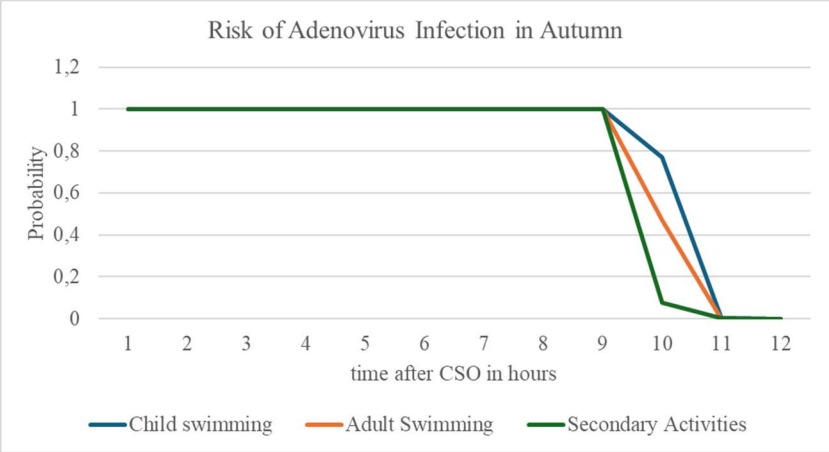

Figure 27: Risk of Adenovirus Infection in Autumn using the maximum values

Lastly in Figure 28 the probability for an Adenovirus infection in winter is displayed. Due to the same speed and direction of the currents as in summer the probability also drops off after about 32 hours.

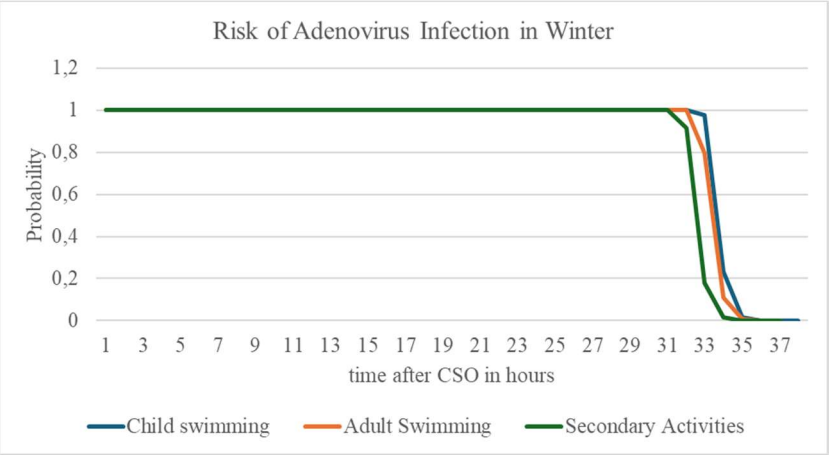

Figure 28: Risk of Adenovirus Infection in Winter using the maximum values

Figure 29 compares the risk of an Adenovirus infection for children swimming for each season. It can be seen that for all seasons the risk remains at 100 % until the pathogens leave the area of the simulation, depending on the speed of the currents.

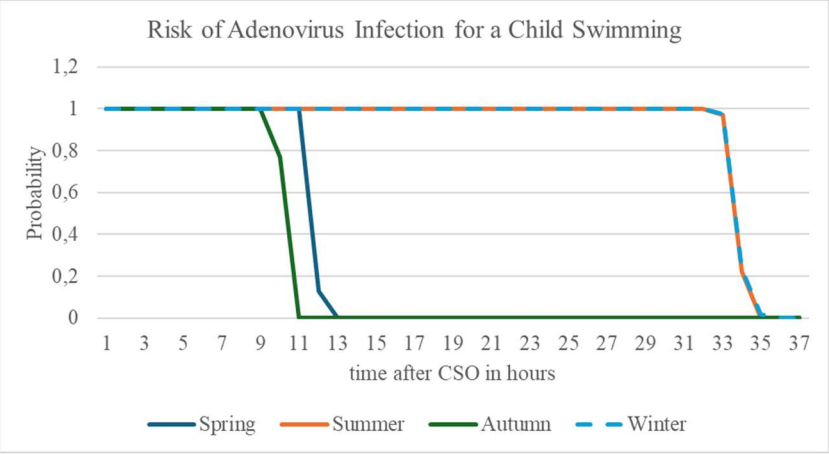

Figure 29: Risk of Adenovirus Infection for a child swimming using the maximum values

The same can be seen in Figure 30 for the risk of an adult swimming, in spring the risk drops after about 12 hours, in autumn after 10 – 11 hours and in summer and winter 33 hours after the CSO.

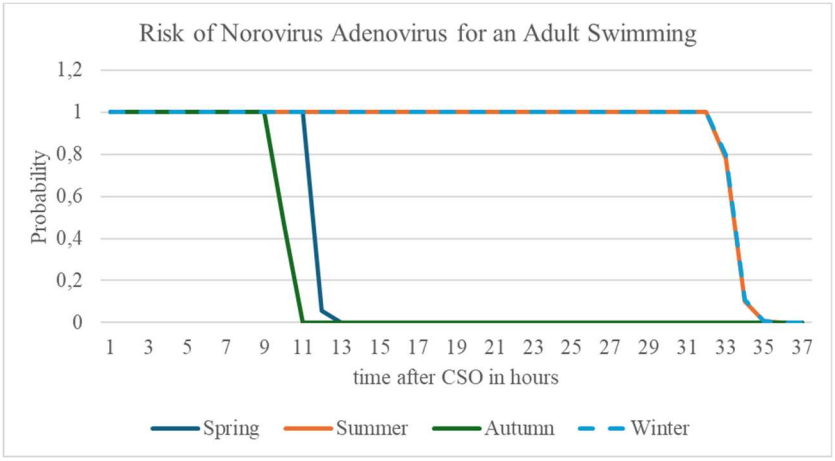

Figure 30: Risk of Adenovirus Infection for an adult swimming using the maximum values

Figure 31 shows the same effect for the risk of an adenovirus infection coming from secondary activities.

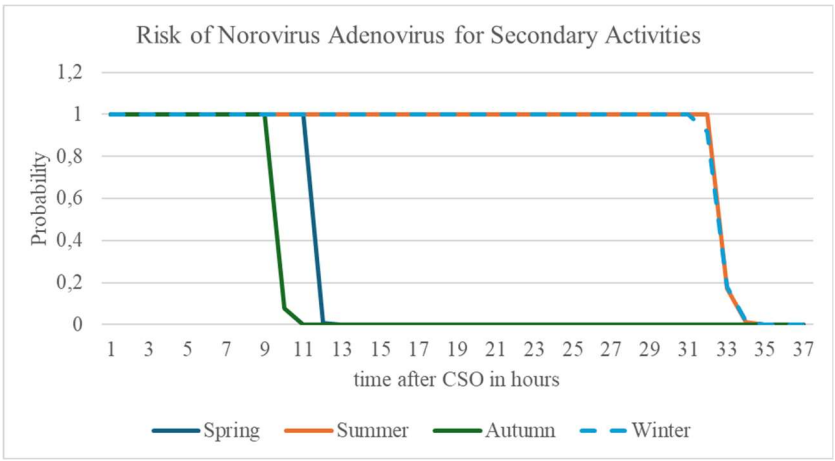

Figure 31: Risk of Adenovirus Infection for secondary activities using the maximum values

In summary, Table 15 shows after which time it is safe again for child to swim following a CSO event for both Norovirus and Adenovirus using a risk threshold of 2 %. Since children ingest the highest amount of water at that point it is also safe for an adult to swim or for people to perform other activities on the water.

Table 15: Times when it is safe for a child to swim after a CSO per season (max. values)

	Spring	Summer	Autumn	Winter
Norovirus	13 h	35 h	11 h	35 h
Adenovirus	13 h	35 h	11 h	35 h

4.2.2. Average values

The average values present a more realistic scenario, with generally lower probabilities of infection compared to the maximum values.

Table 16 and Table 17 show the average probabilities of infection per season after 1, 12, 24 and 36 hours using the average values of pathogen amounts. In this case after 36 hours the probability of all scenarios is already zero and the initial probabilities of infection with Norovirus already start off lower than in the previous case, in a range of 55 – 61 %.

Table 16: Probability of Infection for Spring and Summer using the average values

		Spring			Summer		
Time	Virus	C	A	S	C	A	S
1h	Noro	0,6128	0,5996	0,5648	0,6045	0,5910	0,5555
	Adeno	1	1	1	1	1	1
12h	Noro	0,00011	0	0	0,6036	0,5901	0,5545
	Adeno	0	0	0	1	1	1
24h	Noro	0	0	0	0,4839	0,4663	0,4200
	Adeno	0	0	0	1	1	1
36h	Noro	0	0	0	0	0	0
	Adeno	0	0	0	0	0	0

Table 17: Probability of Infection for Autumn and Winter using the average values

		Autumn			Winter		
Time	Virus	C	A	S	C	A	S
1h	Noro	0,6106	0,5973	0,5623	0,6045	0,5910	0,5556
	Adeno	1	1	1	1	1	1
12h	Noro	0	0	0	0,6039	0,5904	0,5549
	Adeno	0	0	0	1	1	1
24h	Noro	0	0	0	0,4848	0,4672	0,4210
	Adeno	0	0	0	1	1	1
36h	Noro	0	0	0	0	0	0
	Adeno	0	0	0	0	0	0

Figure 32 compares the risk of Norovirus infection for a child swimming for each season using the average values. In spring and autumn, the probability falls below 10 % after 9 hours and 11 hours respectively. In summer and winter this does not happen until 31 hours after the CSO event.

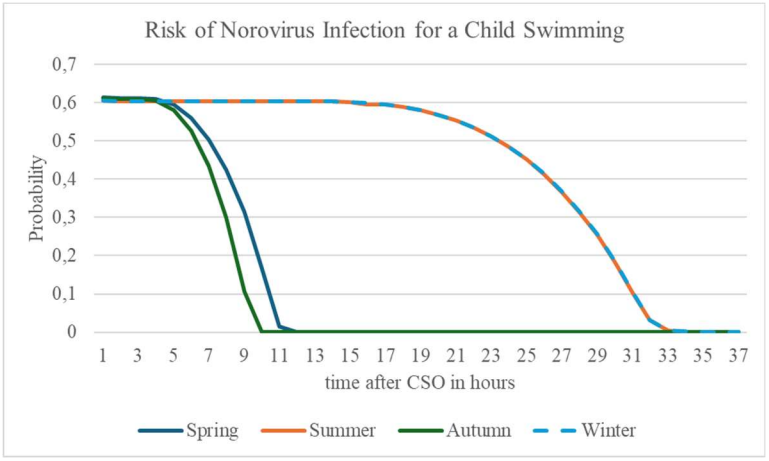

Figure 32: Risk of Norovirus Infection for a child swimming using the average values

The risk of Norovirus infection for an adult swimming in each season are shown in Figure 33 and show basically the same results as in the previous scenario.

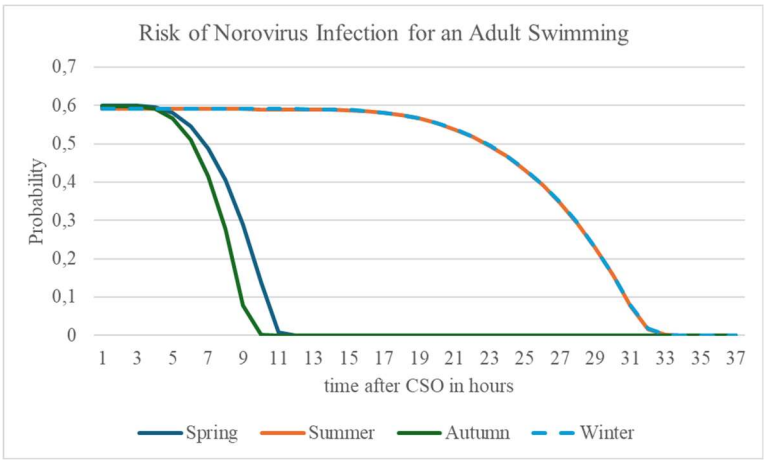

Figure 33: Risk of Norovirus Infection for an adult swimming using the average values

Lastly Figure 34 shows the risk associated with the presence of Norovirus for conducting secondary activities on the water, which again shows the same course for each season.

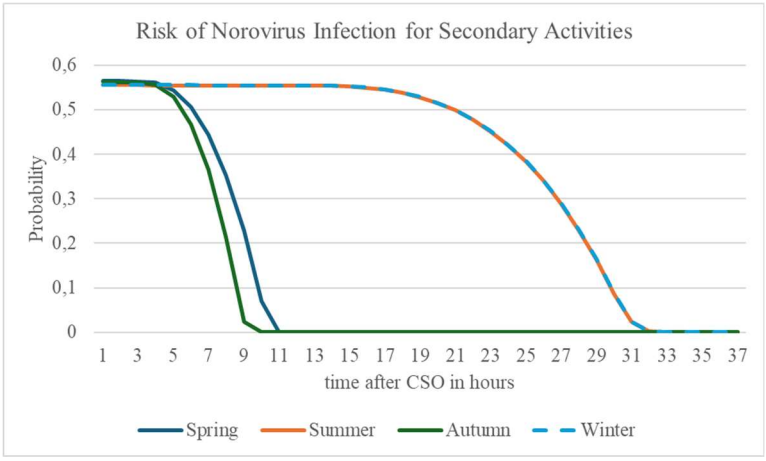

Figure 34: Risk of Norovirus Infection for secondary activities using the maximum values

In Figure 35 the risk of an Adenovirus infection for a child swimming in each season is displayed. Using the average values of pathogen amount shows the same result as the maximum ones did previously. The probability of infection remains at 100 % up until the time where the currents transport the contamination out of the simulated area.

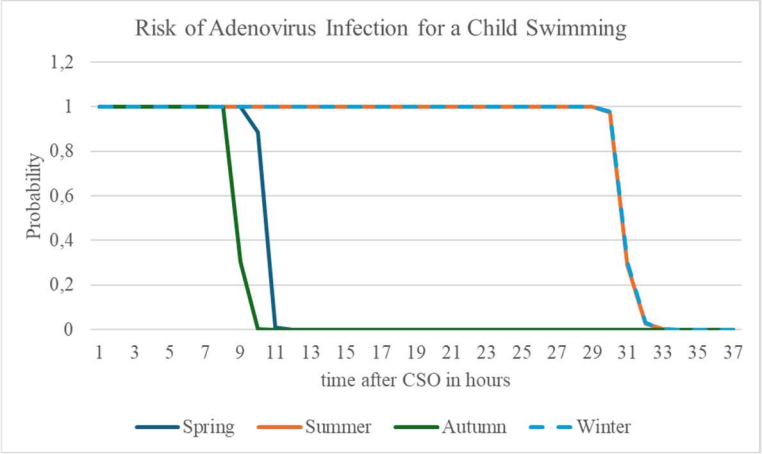

Figure 35: Risk of Adenovirus Infection for a child swimming using the average values

Figure 36 shows the risk of an Adenovirus infection for adults swimming in each season, again showing the same course of the graphs as before. Depending on each season the probability remains at 100 % and drops off steeply when the pathogens leave the area of the simulation.

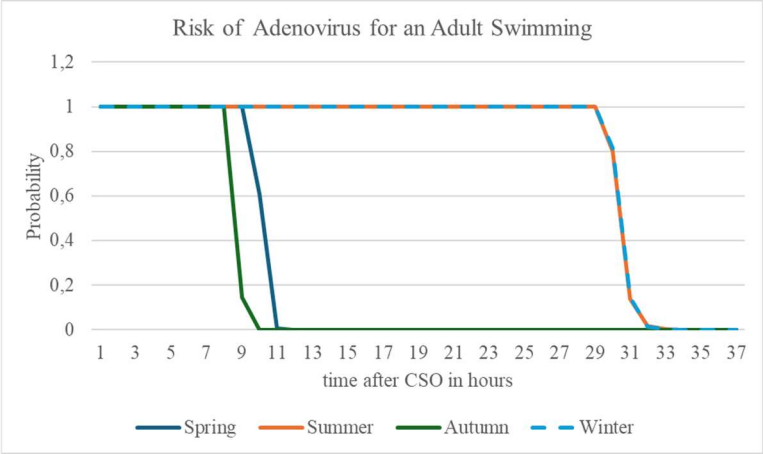

Figure 36: Risk of Adenovirus Infection for an adult swimming using the average values

Lastly Figure 37 displays the risk associated with Adenovirus for people performing secondary activities on the water. Just as before the risk remains at 100% as long as the pathogens are present in the simulated area.

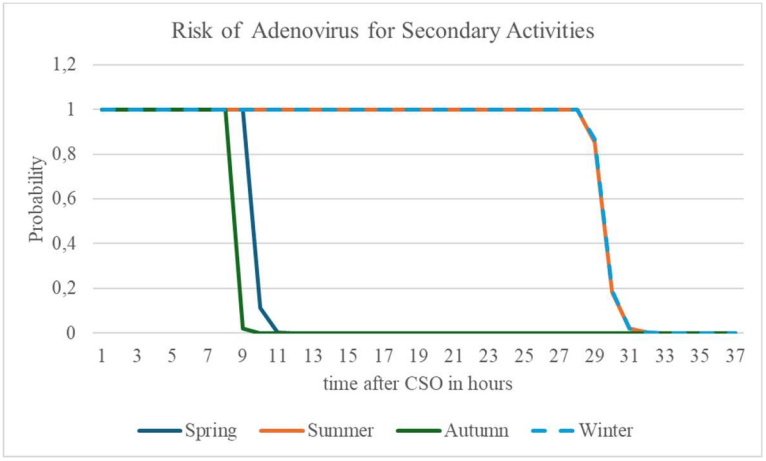

Figure 37: Risk of Adenovirus Infection for secondary activities

Table 18 shows after which time it is safe again for child to swim following a CSO event for both Norovirus and Adenovirus using a risk threshold of 2 %.

Table 18: Times when it is safe for a child to swim after a CSO per season (avg. values)

	Spring	Summer	Autumn	Winter
Norovirus	11 h	33 h	10 h	33 h
Adenovirus	11 h	33 h	10 h	33 h

4.2.3. Comparison

Comparing Table 15 and Table 18 show that the difference between using the maximum or average concentrations of pathogens lead to a time difference of 1 – 2 hours before it is safe for children to swim again after a CSO event using a risk threshold of 2 %.

Figure 38 compares the risk of a Norovirus infection for a child swimming during each season for the maximum and average values. The course of the graphs is parallel, but the average values are continuosly between 10 and 20 % below the probabilities for the maximum values. In summer and winter this leads to a difference of approximately 3 hours for the moment in which the probability of infection is reduced to zero, while in spring and autumn the difference is closer to two hours.

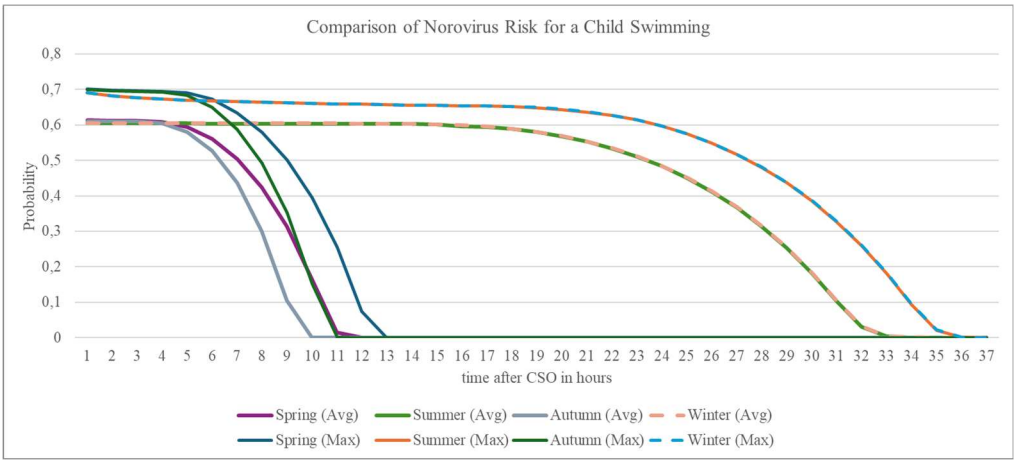

Figure 38: Comparison of Norovirus Risk for a child swimming

The comparison of the risks for a Norovirus infection for an adult swimming in each season for the average and maximum values is shown in Figure 39. Just as in the previous case the probability calculated using the average values lies about 10 – 20 % below the ones from the maximum values and a time offset in the risk reduction of 2 to 3 hours.

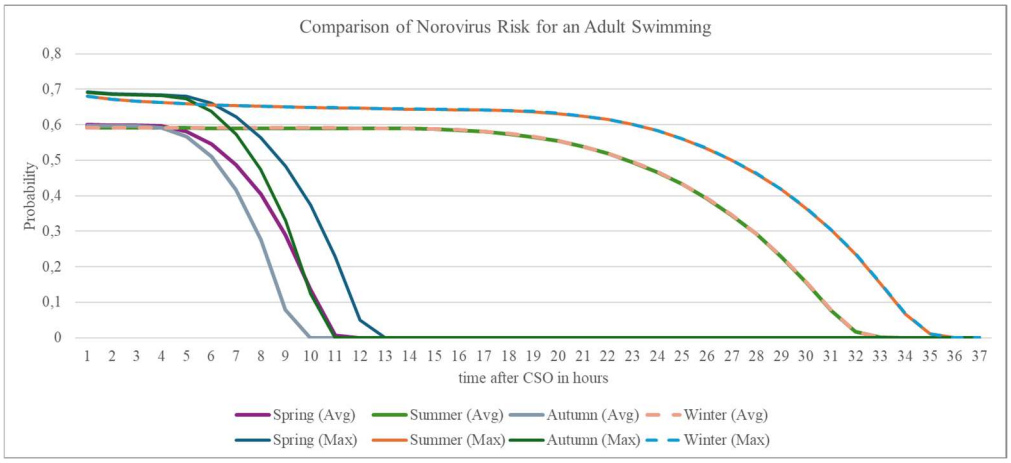

Figure 39: Comparison of Norovirus Risk for an adult swimming

The same results can be seen in Figure 40, which compares the average and maximum values for each season for the risk of a Norovirus infection coming from secondary activities performed on the water.

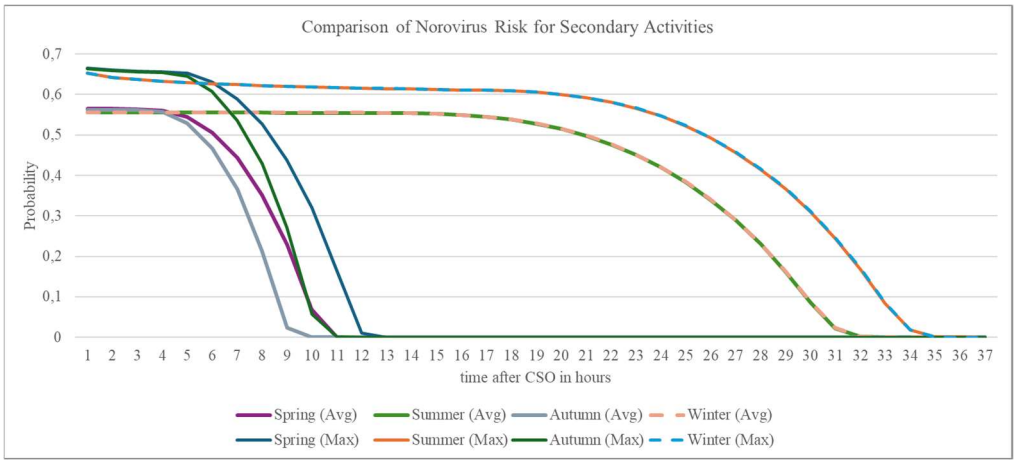

Figure 40: Comparison of Norovirus Risk for secondary activities

Overall, the difference in infection probability for Norovirus between using the maximum and average amounts lies within 10 and 20 %, depending on the time that has passed since the CSO.

Figure 41 compares the risk of an Adenovirus infection for a child swimming for each season for the maximum and average values. Other than with Norovirus in this case the probability of infection remains at 100 % for most of the time in all cases. The drop off at the end of the curve happens with a delay of about 3 hours between the average values in summer and winter, just as in the previous scenario. The time setoff in spring amounts to approximately 1 hour and between 1 and 2 hours in autumn.

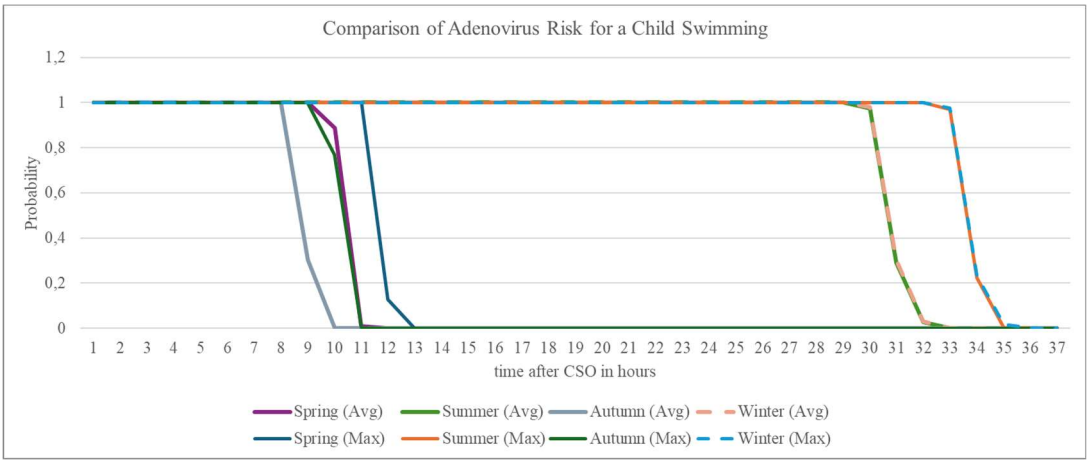

Figure 41: Comparison of Adenovirus Risk for a child swimming

The same results can be seen in Figure 42, showing the same comparison but for the case of an adult swimming.

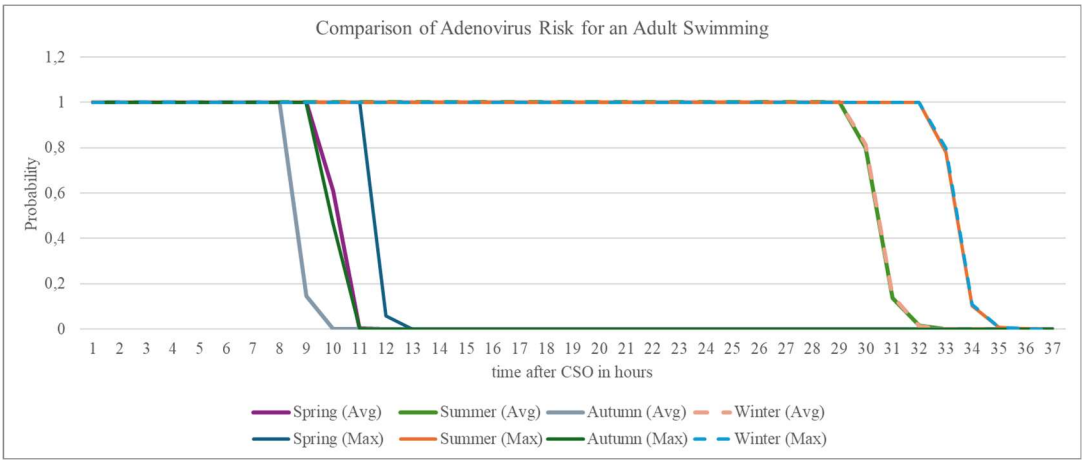

Figure 42: Comparison of Adenovirus Risk for an adult swimming

Lastly Figure 43 compares the same conditions for secondary activities, which gives the same results as the previous cases.

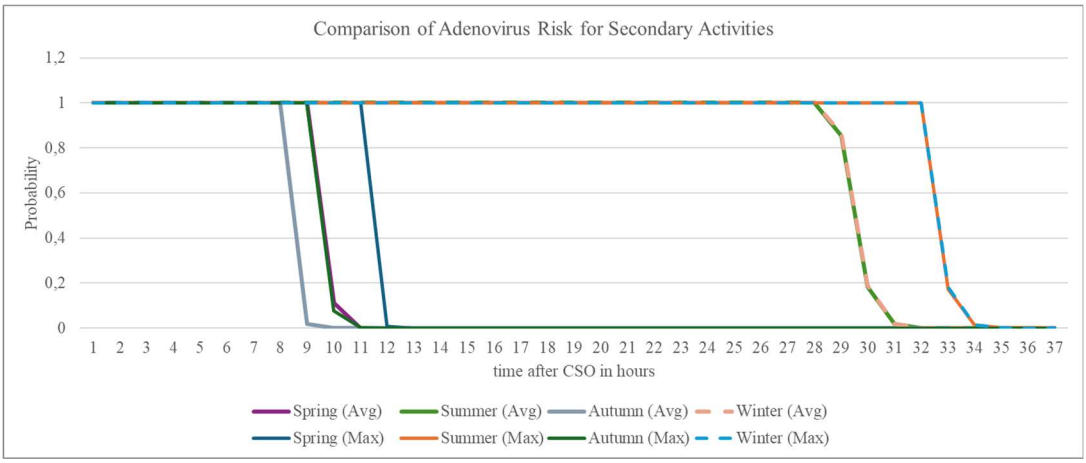

Figure 43: Comparison of Adenovirus Risk for secondary activities

The comparison highlights that while maximum values are critical to understand the worst-case scenarios, using average values may be a more realistic approach to practical risk management and decision making. Since in this case for using the maximum values the time the beach would have to be closed would only be two hours longer than for the scenario using average values, this might be the recommendable approach.

4.3. Impacts of environmental conditions

The results displayed in the previous chapter have shown that the differences in environmental conditions between the scenarios have very little impact on the outcome of the risk assessments. The biggest differences in the outputs were determined by the speed and direction of the sea currents. This is effectively demonstrated by the course of the graphs for summer and winter. Both scenarios have been assessed using the same speed and direction of currents but had the biggest differences in environmental conditions. For the summer scenario a temperature of 23,5 °C and a solar radiation of 285,39 W/m^2 was used, while in winter the conditions included 14,2 °C and 94,82 W/m^2. Despite this the probability of infection in all cases has been almost the same, the difference is usually lower than 1 %.

4.4. Limitations

The biggest limitation of the program is that the depth of the sea is not considered in the pathogen distribution. The spread of pathogens in three instead of just two spatial dimensions would likely lead to a bigger dilution and consequently a lower risk of infection. Also, sea currents can vary throughout different layers of depth, which would heavily impact the distribution as well.

The simulation accounts only for certain environmental parameters, while in reality more factors might come into play. Also, in this case the assumption has been made that one equation can apply to all present FIB, due to the lack of available data in literature to calculate the degradation for each type of FIB separately. Additionally, their effects on the indicator bacteria might not be the same as their effect on the actual pathogens themselves, as has been described in chapter 3.2.1. To improve accuracy, it would be better to consider the environmental impacts on the pathogens themselves and also include more pathogens overall, since there are others present in wastewater than just Norovirus and Adenovirus. The same applies to the conditions on the beach itself, it is not known how long pathogens might survive after being flushed onto the beach. Also, more sample campaigns would be necessary to verify the FIB to pathogen ratios which have been used.

Geographically this simulation only considers the area around Bogatell beach, it does not consider the possible distribution of pathogens to the sea or other beaches in the area. So, a risk reduction on Bogatell beach could mean an increased risk at other beaches in the area, if the contamination is transported in their direction. Also, while the outcome of the risk assessment may show a risk that is too high for swimming, especially during the first hours after the CSO, the pathogens have not yet come close to the beach. A more detailed assessment should include the risk at different point on the beach.

Additionally, the real source of the CSO lies within the breakwater, not at the end like in the simulation. By the time the contamination exits the area of the breakwater the wastewater is already diluted, reducing the pathogen concentration, which would decrease the risk posed to beachgoers. On the other hand, this also means that it likely takes longer for the contamination to be transported by the currents, which could increase the time the beach would have to be closed.

Generally, the equations used for the dose-response model and their associated parameters have a huge impact on the outcome of the risk assessment, depending on how their parameters are chosen the results may vary.

4.5. Impacts of Climate Change

Climate change impacts many aspects which influence the state of the Mediterranean Sea, such as air and water temperature, precipitation, extreme weather events, rising of sea levels, and ocean salinity and acidification [7]. For the sixth Intergovernmental Panel on Climate Change IPCC report AR6 a set of different climate change scenarios have been developed, the so called "Shared Socioeconomic Pathways" SSPs. The SSP1 scenario is considered the "green" scenario with a focus on sustainability. SSP2 describes a scenario in which the past and current global development is extrapolated and environmental systems face some degradation. SSP3 leads to regional rivalry between countries and global inequality increases. In SSP4 there is even more inequality, while some regions focus on local environmental problems in others the environment is severely damaged. Lastly in SSP5 a fossil-fuelled development is considered, including a global energy-intensive lifestyle. From these assumptions four combinations have been developed and globally agreed upon, in which a certain increase in radiation by the year 2100 is associated with each scenario. This results in the four scenarios SSP585, SSP370, SSP245 and SSP216. So, for the SSP5 scenario it is assumed that by 2100 the solar radiation has increased by 8,5 W/m^2, which is the worst-case scenario. For SSP3 an increase of 7 W/m^2 is assumed, 4,5 W/m^2 for SSP2 and 2,6 W/m^2 for SSP1 [54].

4.5.1. Temperature

The average annual temperature of the Mediterranean area has increased by about 1,5 °C by 2020 compared to pre-industrial times. Projections by The Mediterranean Experts on Climate and environmental Change MedECC show that it may rise by an additional 3,8 – 6,5 °C by 2100, depending on the scenario for the emittance of greenhouse gases. The temperature of the sea surface is expected to raise by 1,1 to 3,8 °C, depending on the climate change scenario. Marine heat waves will become more frequent and intense [7].

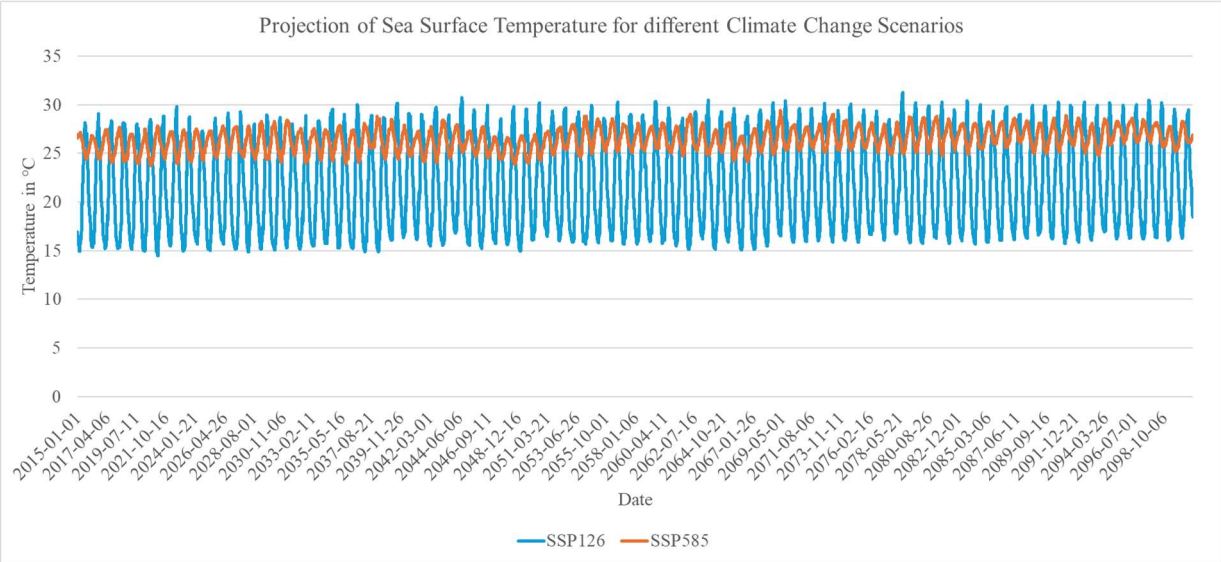

Figure 44: Projection of Sea Surface Temperature for different Climate Change Scenarios between 2015 and 2100 (Data: [14])

Figure 44 shows the projection of the sea surface temperature for the climate change scenarios SSP126 and SSP585, so the best and worst-case scenarios, based on the data from Lobelia Earth [14] using the ACCESS Earth System Model version 1.5, developed by the Australian Commonwealth Scientific and Industrial Research Organisation (CSIRO) and the Australian Bureau of Meteorology (BoM). For the SSP126 scenario the sea surface temperature is projected to fluctuate between 15 °C and 27 °C, while for the SSP585 case the range is narrowed down a lot to 24 °C to 27 °C throughout the year.

4.5.2. Acidification

According to research by Hassoun et al. the levels of CO_2 in the atmosphere have increased to over 420 ppm in 2022, which is almost 50 % higher than before the industrialization. Most of it comes from anthropogenic activities, including the use of fossil fuels and deforestation. From 1800 to 1994 about half the anthropogenic CO_2 has been absorbed by the oceans, which act as a CO_2-sink. This adsorption ultimately leads to a pH decrease, so an acidification of the seas [55]. The oceans absorb about 30 % of anthropogenic carbon [7].

The warm, alkaline water of the Mediterranean Sea can easily absorb CO_2 from the atmosphere and has a higher concentration of anthropogenic carbon than the global average, due to its alkaline conditions and a more frequent overturning and ventilation of deeper water layers [7], [56]. In the Mediterranean Sea the Western basin has been shown to accumulate more anthropogenic carbon than the Eastern Basin [56]. From pre-industrial times to 2013 the acidification falls in the range of -0,055 to -0,156 pH units, reflecting the CO_2-increase in the atmosphere and the following absorption of CO_2 by the oceans [56]. By 2100 the pH of the Western basin may be reduced by up to 0,462 pH units [7].

The increasing acidification improves the survival conditions for FIB (chapter **Fehler! Verweisquelle konnte nicht gefunden werden.**) and possibly of the related pathogens as well.

4.5.3. Rainfall

According to the MedECC since the 1950s rainfalls have decreased in frequency and amount especially during winter. Projections show that precipitation in the Mediterranean Area is going to continue decreasing by about 4 % per degree of global warming. While the overall amount of precipitation is going to decrease more extreme weather events are going to become more frequent [7]. More frequent heavy rains may also lead to more frequent CSO events.

4.5.4. UV Radiation

Since the 1980s solar radiation has increased in the Mediterranean basin, an increase ranging between 0,9 and 4,6 W/m2 per decade [7]. According to MedECC predictions due to the decrease of anthropogenic aerosol levels solar radiation is going to raise further [7]. As described in previous chapters UV radiation seemed to have negative impact on microbial survival in water, so this might slightly reduce the pathogen survival in water. Although it has been shown the impact of environmental conditions on the outcomes of the risk assessment has been rather small.

4.5.5. Salinity

For the impact of climate change on sea salinity there are different projections available in literature. According to Cramer et al. the salinity in the Mediterranean Sea is likely going to vary at different times and in different areas [7].

Figure 45 shows the projection of sea surface salinity for the four climate change scenarios based on the data from Lobelia Earth [14]. The decrease in sea surface salinity is likely related to the melting of the pole caps, which will progress faster for the other scenarios than for

SSP126. The increase in fresh water from the melted ice decreases the overall salinity of the oceans [57].

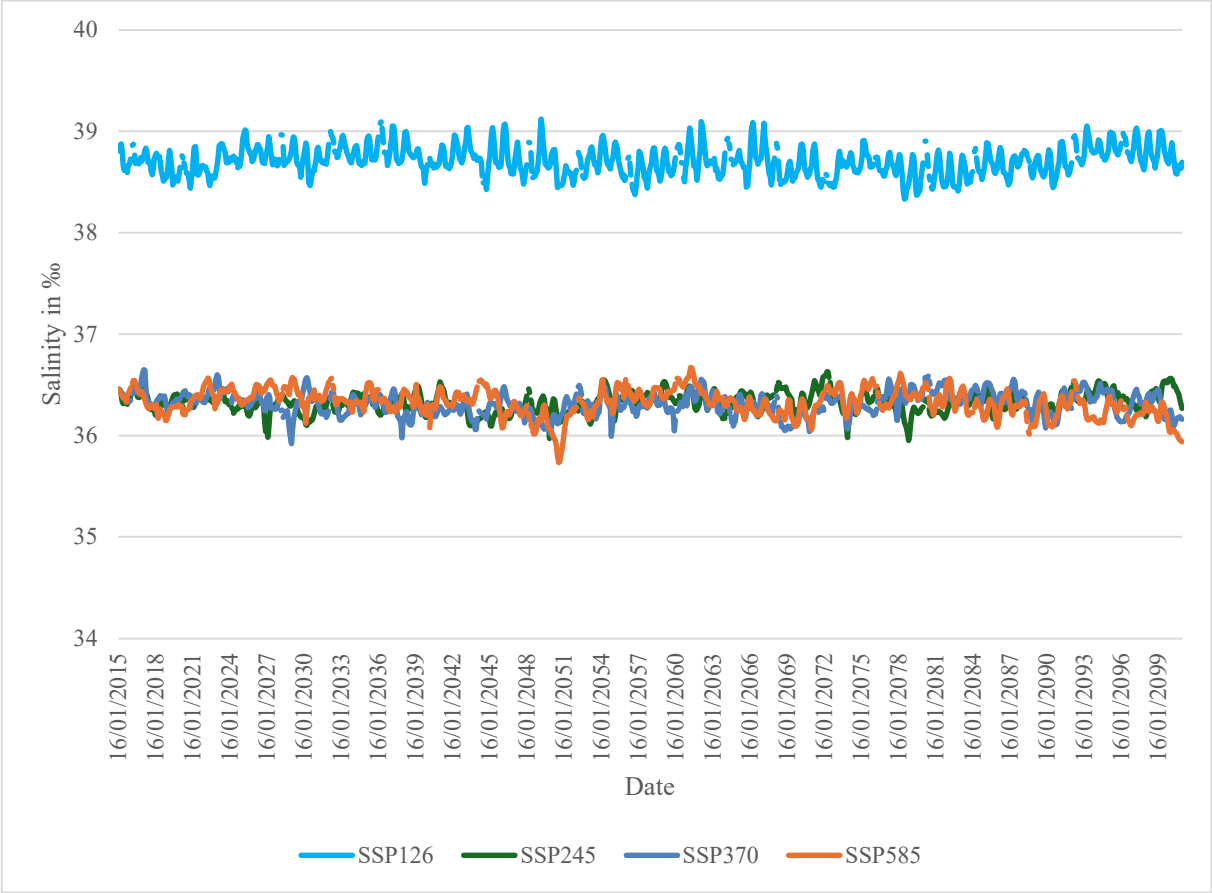

Figure 45: Projection of Sea Surface Salinity for different Climate Change Scenarios between 2015 and 2100 (Data: [14])

Other studies on the other hand suggest an increase in salinity for the Mediterranean Sea. According to Soto-Navarro et al. the salinity may increase due to a lower input of freshwater coming from the reduced amounts of rain and subsequently less river runoff [58]. All in all, since there is currently no reliable concrete estimation on the impact of climate change on sea salinity that would enable any prediction on how it may influence pathogen survival in the ocean.

4.5.6. Sea currents

According to Calvo et al. the changes in salinity and temperature in the Mediterranean Sea impact the density of layers of different density, which could possibly alter the patterns of the sea currents as well. The density has a bigger impact than wind speed and directions on the currents [16].

5. CONCLUSIONS

The primary objective of this thesis was to model the quantitative microbiological risk assessment in bathing waters at Bogatell beach in Barcelona after CSO events under varying environmental conditions. It included assessing the influence of different environmental parameters and the possible future impacts of climate change on pathogen concentrations and the associated health risks. This project has successfully provided a detailed simulation and analysis of these factors, creating insights into human health risks associated with recreational water use after CSOs.

Through the development and implementation of a simulation model using Python, the distribution and degradation of faecal indicator bacteria were analysed across different seasons. The results highlight that sea currents, rather than environmental conditions such as temperature or sunlight, play a predominant role in determining the distribution of pathogens following a CSO event. The simulations indicated that during summer and winter, the currents directed pathogens towards the beach, which increased the risk of infection for beachgoers. In contrast, during spring and autumn, the currents carried the contamination parallel to the beach, reducing direct exposure risk on the beach, but possibly posing a risk to beaches in the surrounding area.

The risk assessment considered three different scenarios: a child swimming, an adult swimming, and a person engaged in secondary water activities such as kayaking or rowing. During the risk assessment the risks using both maximum and average pathogen concentrations were compared. The findings revealed that the probability of infection was higher when using maximum values, the difference in infection probability generally lies within 10 % to 20 %, but overall, the time difference for which the beach would have to be closed in both scenarios amounted to one to two hours. Generally, the risk for a Norovirus infection was the highest directly after the CSO event, with probabilities ranging between 65 % and 70 %, while the risk for Adenovirus infection started at 100 % across all scenarios and was only reduced by the contamination being transported out of the simulated area.

The impact of environmental conditions, including temperature and solar radiation, was found to be minimal on the overall risk assessment outcomes. This reinforces the conclusion that sea currents are the dominant factor influencing pathogen spread and consequently the risk of infection. Additionally, several limitations were identified, such as the assumption of uniform degradation rates for all types of FIB depending on environmental conditions and that it is unknown how long pathogens which got flushed onto the beach may survive there and pose a potential risk to people. These limitations suggest that future studies should incorporate a broader range of environmental factors and pathogen-specific degradation rates to enhance model accuracy.

The influence of climate change was also considered, focusing on projections of sea temperature, acidification, and salinity under different Shared Socioeconomic Pathways (SSP) scenarios. Climate change could also possibly alter sea current patterns, further impacting pathogen distribution and associated health risks. However, the precise effects remain uncertain, necessitating ongoing research to refine these projections and develop adaptive management strategies.

These findings underscore the need for robust monitoring systems and adaptive risk management frameworks to mitigate health risks associated with CSO events and climate change impacts.

Moreover, this research highlights the critical role of interdisciplinary approaches in addressing complex environmental health issues. Collaboration between hydrologists, microbiologists, environmental engineers, and public health officials is essential to develop

integrated solutions that can effectively manage and mitigate risks. The application of advanced computational tools, like a simulation in Python used in this project, demonstrates the potential of technology in enhancing the understanding and management of environmental health risks.

Future work should focus on refining the QMRA model by incorporating more on-site data, verify the used pathogen to indicator ratios and include assumptions for the pathogen survival on the beach to increase the accuracy of the simulation. Expanding the scope to include a wider range of pathogens and environmental conditions will also provide a more comprehensive risk assessment framework.

6. REFERENCES

[1] D. A. Holcomb and J. R. Stewart, "Microbial Indicators of Fecal Pollution: Recent Progress and Challenges in Assessing Water Quality," *Current Environmental Health Reports*, vol. 7, no. 3. Springer, pp. 311–324, Sep. 01, 2020. doi: 10.1007/s40572-020-00278-1.

[2] E. Sokolova, "Hydrodynamic and Microbiological Modelling of Water Quality in Drinking Water Sources," Chalmers University of Technology, Gothenburg, Swedeen, 2011. [Online]. Available: www.chalmers.se

[3] A. Korajkic, B. R. McMinn, and V. J. Harwood, "Relationships between microbial indicators and pathogens in recreational water settings," *International Journal of Environmental Research and Public Health*, vol. 15, no. 12. MDPI, Dec. 13, 2018. doi: 10.3390/ijerph15122842.

[4] Instituto Nacional de Estadística, "Population of the Continuous Municipal Register by Population Unit." Accessed: Jun. 07, 2024. [Online]. Available: https://www.ine.es/nomen2/index.do?accion=busquedaAvanzada&entidad_amb=no&codProv=08&codMuni=19&codEC=0&codES=0&codNUC=0&denominacion_op=like&denominacion_txt=&L=1

[5] E. Gutiérrez, P. Malgrat, D. Suñer, and P. Otheguy, "Real Time Management of Bathing Water Quality in Barcelona," 2010. [Online]. Available: https://hal.science/hal-03296508

[6] D. Saurí and L. Palau-Rof, "Urban Drainage in Barcelona: From Hazard to Resource?," Barcelona, Spain, 2017. [Online]. Available: www.water-alternatives.org

[7] W. Cramer, K. Marini, and J. Guiot, "CLIMATE AND ENVIRONMENTAL CHANGE IN THE MEDITERRANEAN BASIN Current situation and risks for the future First Mediterranean Assessment Report by MedECC (Mediterranean Experts on Climate and environmental Change)."

[8] G. Cembrano[o], J. Figueras[o], J. Quevedo, V. Puig, M. Salamero, and J. Martí, "GLOBAL CONTROL OF THE BARCELONA SEWERAGE SYSTEM FOR ENVIRONMENT PROTECTION," 2002. [Online]. Available: www.elsevier.com/locate/ifac

[9] A. O. Sojobi and T. Zayed, "Impact of sewer overflow on public health: A comprehensive scientometric analysis and systematic review," *Environmental Research*, vol. 203. Academic Press Inc., Jan. 01, 2022. doi: 10.1016/j.envres.2021.111609.

[10] Google, "Google Maps Bogatell Beach Barcelona," Google Maps. Accessed: Jun. 07, 2024. [Online]. Available: https://maps.app.goo.gl/j3wdpxZXXFif8zMV9

[11] F. E. Eregno, I. Tryland, T. Tjomsland, M. Myrmel, L. Robertson, and A. Heistad, "Quantitative microbial risk assessment combined with hydrodynamic modelling to estimate the public health risk associated with bathing after rainfall events," *Science of the Total Environment*, vol. 548–549, pp. 270–279, Apr. 2016, doi: 10.1016/j.scitotenv.2016.01.034.

[12] EUROPEAN COMMISSION European Climate Infrastructure and Environment Executive Agency, "DYNAMIC INFORMATION MANAGEMENT APPROACH FOR THE IMPLEMENTATION OF CLIMATE RESILIENT ADAPTATION PACKAGES IN EUROPEAN REGIONS," *GRANT AGREEMENT NUMBER 101037084 — IMPETUS*. 2021. doi: 10.3030/101037084.

[13] C. Bosch, "Advanced urban water management to efficiently ensure bathing water quality," https://webgate.ec.europa.eu/life/publicWebsite/project/LIFE17-ENV-ES-000396/advanced-urban-water-management-to-efficiently-ensure-bathing-water-

quality. Accessed: Jun. 07, 2024. [Online]. Available: https://webgate.ec.europa.eu/life/publicWebsite/project/LIFE17-ENV-ES-000396/advanced-urban-water-management-to-efficiently-ensure-bathing-water-quality

[14] Lobelia Earth and V. Estella-Perez, "Weather Data at Barcelona Airport provided by Lobelia Earth," *Datos climáticos para task 4.8.1*. 2024.

[15] Instituto de Estadística de Cataluña, "Agua del mar. Temperatura media. A diferentes profundidades," Agua del mar. Temperatura media anual. Por meses i diferentes profundidades Cataluña. 2022. Accessed: Jun. 07, 2024. [Online]. Available: https://www.idescat.cat/indicadors/?id=aec&n=15196&lang=es

[16] E. Calvo *et al.*, "Effects of climate change on Mediterranean marine ecosystems: The case of the Catalan Sea," *Climate Research*, vol. 50, no. 1. pp. 1–29, Dec. 01, 2011. doi: 10.3354/cr01040.

[17] J. Martínez *et al.*, "Atlas of surface currents in the Mediterranean and Canary–Iberian–Biscay waters," *Journal of Operational Oceanography*, vol. 17, no. 1, pp. 40–62, 2024, doi: 10.1080/1755876X.2022.2102357.

[18] E. García Ladona, J. Ballabrera, C. González, J. Martínez, F. Pérez, and A. García Espriu, "COSMO Site," https://cosmo.icm.csic.es/. Accessed: Jun. 07, 2024. [Online]. Available: https://cosmo.icm.csic.es/

[19] European Union, "Program Summary of Interreg Euro-MED Co-founded by the European Union." Accessed: Jun. 07, 2024. [Online]. Available: https://interreg-euro-med.eu/en/documents-tools-programme-documents

[20] A. B. Boehm and L. M. Sassoubre, "Enterococci as Indicators of Environmental Fecal Contamination," 2014. [Online]. Available: https://www.ncbi.nlm.nih.gov/books/

[21] E. Sokolova, J. Åström, T. J. R. Pettersson, O. Bergstedt, and M. Hermansson, "Decay of bacteroidales genetic markers in relation to traditional fecal indicators for water quality modeling of drinking water sources," *Environ Sci Technol*, vol. 46, no. 2, pp. 892–900, Jan. 2012, doi: 10.1021/es2024498.

[22] R. A. Blaustein, Y. Pachepsky, R. L. Hill, D. R. Shelton, and G. Whelan, "Escherichia coli survival in waters: Temperature dependence," *Water Res*, vol. 47, no. 2, pp. 569–578, Feb. 2013, doi: 10.1016/j.watres.2012.10.027.

[23] C. N. Haas, J. B. Rose, and C. P. Gerba, "QUANTITATIVE MICROBIAL RISK ASSESSMENT."

[24] M. Hussain, S. Ajaz Rasool, M. Tanweer Khan, and A. Wajid, "ENTEROCOCCI VS COLIFORMS AS A POSSIBLE FECAL CONTAMINATION INDICATOR: BASELINE DATA FOR KARACHI," 2007.

[25] Eurecat, "Eurecat Report on IMPETUS WP4_T4.8.1_Technical Report M18_EUT_v1," *Eurecat Report on Task 4.8.1*.

[26] M. Solic and N. Krstulovic, "Separate and Combined Effects of Solar Radiation, Temperature, Salinity and pH on the Survival of Faecal Coliforms in Seawater," Split, Croatia, 1992.

[27] J. L. Mancini, "Numerical Estimates of Coliform Mortality Rates under Various Conditions," 1978. Accessed: Jun. 07, 2024. [Online]. Available: https://www.jstor.org/stable/25040179

[28] G. Martinez *et al.*, "Using the Q10 model to simulate E. coli survival in cowpats on grazing lands," *Environ Int*, vol. 54, pp. 1–10, 2013, doi: 10.1016/j.envint.2012.12.013.

[29] Y. A. Pachepsky, R. A. Blaustein, G. Whelan, and D. R. Shelton, "Comparing temperature effects on Escherichia coli, Salmonella, and Enterococcus survival in

surface waters," *Lett Appl Microbiol*, vol. 59, no. 3, pp. 278–283, 2014, doi: 10.1111/lam.12272.

[30] A. Tiwari *et al.*, "Effects of temperature and light exposure on the decay characteristics of fecal indicators, norovirus, and Legionella in mesocosms simulating subarctic river water," *Science of the Total Environment*, vol. 859, Feb. 2023, doi: 10.1016/j.scitotenv.2022.160340.

[31] Y. Rozen and S. Belkin, "Survival of enteric bacteria in seawater: Table 1," *FEMS Microbiol Rev*, vol. 25, no. 5, pp. 513–529, Dec. 2001, doi: 10.1111/j.1574-6976.2001.tb00589.x.

[32] T. Lacoue-Labarthe *et al.*, "Impacts of ocean acidification in a warming Mediterranean Sea: An overview," *Reg Stud Mar Sci*, vol. 5, pp. 1–11, May 2016, doi: 10.1016/j.rsma.2015.12.005.

[33] M. R. Hipsey, J. P. Antenucci, and J. D. Brookes, "A generic, process-based model of microbial pollution in aquatic systems," *Water Resour Res*, vol. 44, no. 7, Jul. 2008, doi: 10.1029/2007WR006395.

[34] O. B. Yalcin and A. Muhammetoglu, "Modelling inactivation rates of indicator microorganisms based on laboratory determinations of T90 for different temperature and salinity levels," *Desalination Water Treat*, vol. 26, no. 1–3, pp. 45–52, 2011, doi: 10.5004/dwt.2011.2108.

[35] R. C. Feitosa, P. C. C. Rosman, J. L. B. Carvalho, M. B. V. Côrtes, and J. C. Wasserman, "Comparative study of fecal bacterial decay models for the simulation of plumes of submarine sewage outfalls," *Water Science and Technology*, vol. 68, no. 3, pp. 622–631, 2013, doi: 10.2166/wst.2013.286.

[36] L. W. Sinton, C. H. Hall, P. A. Lynch, and R. J. Davies-Colley, "Sunlight inactivation of fecal indicator bacteria and bacteriophages from waste stabilization pond effluent in fresh and saline waters," *Appl Environ Microbiol*, vol. 68, no. 3, pp. 1122–1131, 2002, doi: 10.1128/AEM.68.3.1122-1131.2002.

[37] Agencia Estatal de Meteorología AEMET - Gobierno de España, "AEMET OpenData," https://www.aemet.es/es/datos_abiertos/AEMET_OpenData. Accessed: Jun. 07, 2024. [Online]. Available: https://www.aemet.es/es/datos_abiertos/AEMET_OpenData

[38] A. - Agència de Salut Pública de Barcelona, "Informe de la qualitat sanitària de l'aigua de bany de les platges de Barcelona 2017," 2017.

[39] A. Llopart-Mascaró Bassols, "Barcelona CSO Data," *Servei Ambiental i Relacions Externes Direcció de Planificació i Innovació Barcelona Cicle de l'Aigua, SA Serveis Urbans i Manteniment de l'Espai Públic Ajuntament de Barcelona*.

[40] M. Rusiñol, "Informe resultats anàlisi mostres aigua de mar projecte IMPETUS from Eurecat," *Laboratori de virus contaminants d'aigua i aliments (VIRCONT) Secció de Microbiologia, Virologia i Biotecnologia Departament de Genètica, Microbiologia i Estadística Facultat Biologia Universitat Barcelona* . 2024.

[41] C. Torres Costa, "Data on Pathogen Indicator Ratios from the iBathwater project from Eurecat," *Pathogen Ratios in iBathwater from Eurecat*.

[42] R. Periáñez, *Modelling the Dispersion of Radionuclides in the Marine Environment - An Introduction*. Springer-Verlag Berlin Heidelberg, 2005.

[43] Python Software Foundation, "What is Python? Executive Summary ," https://www.python.org/doc/essays/blurb/. Accessed: Jun. 07, 2024. [Online]. Available: https://www.python.org/doc/essays/blurb/

[44] R. B. Bird, W. E. Stewart, and E. N. Lightfood, *Transport Phenomena*, Second Edition. John Wiley & Sons, Inc.

[45] A. DeCaria, "ESCI 340-Cloud Physics and Precipitation Processes Lesson 6-Growth of Cloud Droplets by Diffusion." Millersville University. Accessed: Jun. 08, 2024. [Online]. Available: https://www.atmos.millersville.edu/~adecaria/ESCI340/esci340-Lesson06-Diffusional-Growth.pdf

[46] E. L. Cussler, *Diffusion Mass Transfer in Fluid Systems*, Third Edition. Cambridge University Press, 2009. [Online]. Available: www.cambridge.org/cussler.

[47] I. Federigi, M. Verani, G. Donzelli, L. Cioni, and A. Carducci, "The application of quantitative microbial risk assessment to natural recreational waters: A review," *Marine Pollution Bulletin*, vol. 144. Elsevier Ltd, pp. 334–350, Jul. 01, 2019. doi: 10.1016/j.marpolbul.2019.04.073.

[48] World Health Organization WHO, *Quantitative Microbial Risk Assessment: Application for Water Safety Management*. 2016. [Online]. Available: http://www.who.

[49] A. P. Dufour, T. D. Behymer, R. Cantú, M. Magnuson, and L. J. Wymer, "Ingestion of swimming pool water by recreational swimmers," *J Water Health*, vol. 15, no. 3, pp. 429–437, Jun. 2017, doi: 10.2166/wh.2017.255.

[50] C. A. Dada and J. Cooke, "Quantitative Microbial Risk Assessment (QMRA) of the Pōrangahau Wastewater Treatment Plant discharge," 2022.

[51] J. Mitchell and M. Weir, "QMRA Wiki of the Michigan State University, College of Engineering, Department of Biosystems and Agricultural Engineering," Adenovirus. Accessed: Jun. 07, 2024. [Online]. Available: https://qmrawiki.org/pathogens/adenovirus

[52] V. N. Chigor, T. Sibanda, and A. I. Okoh, "Assessment of the Risks for Human Health of Adenoviruses, Hepatitis A Virus, Rotaviruses and Enteroviruses in the Buffalo River and Three Source Water Dams in the Eastern Cape," *Food Environ Virol*, vol. 6, no. 2, pp. 87–98, 2014, doi: 10.1007/s12560-014-9138-4.

[53] U. Fsis, "MICROBIAL RISK ASSESSMENT GUIDELINE PATHOGENIC MICROORGANISMS WITH FOCUS ON FOOD AND WATER Prepared by the Interagency Microbiological Risk Assessment Guideline Workgroup," 2012.

[54] M. Böttinger and D. Kasang, "The SSP Scenarios by the DKRZ Deutsche Klimarechenzentrum," The SSP Scenarios.

[55] A. E. R. Hassoun *et al.*, "Ocean acidification research in the Mediterranean Sea: Status, trends and next steps," *Frontiers in Marine Science*, vol. 9. Frontiers Media S.A., Sep. 27, 2022. doi: 10.3389/fmars.2022.892670.

[56] A. E. R. Hassoun *et al.*, "Acidification of the Mediterranean Sea from anthropogenic carbon penetration," *Deep Sea Res 1 Oceanogr Res Pap*, vol. 102, pp. 1–15, Aug. 2015, doi: 10.1016/j.dsr.2015.04.005.

[57] Center for Science Education UCAR, "How Melting Arctic Ice Affects Ocean Currents," How Melting Arctic Ice Affects Ocean Currents by Center for Science Education UCAR. Accessed: Jun. 08, 2024. [Online]. Available: https://scied.ucar.edu/learning-zone/climate-change-impacts/melting-arctic-sea-ice-and-ocean-currents#:~:text=The%20melting%20ice%20causes%20freshwater,caused%20the%20currents%20to%20slow.

[58] J. Soto-Navarro *et al.*, "Evolution of Mediterranean Sea water properties under climate change scenarios in the Med-CORDEX ensemble," *Clim Dyn*, vol. 54, no. 3–4, pp. 2135–2165, Feb. 2020, doi: 10.1007/s00382-019-05105-4.